3D morphology and timing of the giant fossil pockmark of Beauvoisin, SE Basin of France

Aurélien Gay[1]*, Michel Lopez[1], Jean-Luc Potdevin[2], Valérie Vidal[3], German Varas[4], Alexiane Favier[1,5] & Nicolas Tribovillard[2]

[1] Géosciences Montpellier, UMR CNRS 5243, Université de Montpellier, F-34095 Montpellier, France
[2] Laboratoire d'Océanologie & Géosciences, UMR CNRS 8187, Université de Lille 1, F-59655 Villeneuve d'Ascq, France
[3] Laboratoire de Physique, ENS de Lyon, CNRS, Université de Lyon, F-69342 Lyon, France
[4] Instituto de Física, Pontificia Universidad Católica de Valparaíso, Av. Universidad 330, Valparaíso, Chile
[5] Géoazur Nice, UMR CNRS 7329, Université de Nice–Sophia Antipolis, F-06560 Valbonne, France

A.G., 0000-0003-2003-6679; J.-L.P., 0000-0001-6061-4555; V.V., 0000-0002-0413-1601; A.F., 0000-0002-8508-4762; N.T., 0000-0003-3493-5579
* Correspondence: aurelien.gay@umontpellier.fr

Abstract: The resolution of data acquired over modern seafloors does not allow imaging of the inner features of a fluid seep structure, particularly in the shallow subsurface. In the SE Basin of France (Drôme), fossil cold seep structures comprising fossil-rich carbonate lenses were identified about 30 years ago within the Oxfordian (Late Jurassic) Terres Noires Formation. These structures were first interpreted as pseudo-bioherms related to hydrothermal activity, but comparison with active seep sites on modern margins, together with isotopic analyses, led to a reinterpretation involving cold fluids instead. To date, all seep sites have generally been studied individually without considering any link to neighbouring or more distant sites. Based on 23 high-resolution stratigraphic logs within the structure coupled to mosaicked aerial photographs from a drone survey, 19 fluid seep events were correlated in the area, including two new sites exposed as a result of weathering. We have shown that each identified sub-site is composed of subvertically stacked fossil-rich carbonate lenses interbedded with marls, which developed in smooth, 4–6 m deep depressions beneath the local seabed. The nodules present within the depressions are of primary importance as they mark the area of active seeping. This general organization is very similar to the modern Regab giant pockmark in the Lower Congo Basin where only a few sub-sites are active at the same time. A spatio-temporal 3D reconstruction of the position of these sub-sites shows that the carbonate lenses are organized into clusters comprising up to seven sub-sites grouped together in the same stratigraphic interval and the same geographical zone. A sandbox experiment where gas is injected at constant flow rate at the base of a box filled with a matrix of water-saturated grains displays a pattern consisting of disturbed sediments inside a parabolic-shaped area. This parabolic shape was also identified on a seismic profile across the Regab giant pockmark, suggesting that the processes are similar for the Beauvoisin and Regab seep areas. The laboratory experiments also show that the seeping conduit is stable during a given period of time and suddenly shifts laterally. This is mainly as a result of the collapse of the conduit, the lateral migration and the reopening at a new position. The general log obtained in the Beauvoisin seep area suggests a similar pattern with periods of seeping alternating with periods of quiescence, each of which is *c*. 200 kyr. Even if a pockmark seems to have been inactive for a long period of time, this could be due to the lateral shift of the feeder conduit, meaning that the sub-seafloor is still charged with gas. This is of primary importance for risk assessment, hydrocarbon exploration and general understanding of geobiology at seafloor seeps.

Received 15 March 2018; **revised** 13 September 2018; **accepted** 13 September 2018

Hydrogen sulphide and methane that sustain highly specialized chemosynthetic-based ecosystems in cold seep environments have been recognized in many modern basins worldwide (Campbell 2006; Amano *et al.* 2010; Teichert & van de Schootbrugge 2013) and in the fossil record in the early Cenozoic and onwards (Campbell & Bottjer 1995*b*; Kiel & Little 2006; Kiel 2010; Vrijenhoeck 2013). Sulphide and methane release results in carbonate precipitation forming lenses encased in surrounding limestones or marlstones (Campbell *et al.* 2002). These fossil organism-rich, authigenic, carbonate rocks developed at the seafloor where oil and/or gas migrated from an underlying network of focused fluid flow in sedimentary basins (Bohrmann *et al.* 1998; Aloisi *et al.* 2000, 2002; Gay & Migeon 2017). The fossils dominated by lucinid bivalves generally show larger dimensions than at other sites as they rely on chemotrophic symbionts for nutrition (Paull *et al.* 1992). This biogeochemical process mainly relies on anaerobic oxidation of methane (AOM) (Boetius *et al.* 2000), where the symbiotic consortia of sulphate-reducing bacteria and methanotrophic archaea use both sulphate and

methane for their metabolism and biomass synthesis, thus supplying energy and nutriments to their hosts (Knittel & Boetius 2009; Deusner *et al.* 2014). However, fossil-rich carbonate assemblages have always been considered as individual seep sites without comparing their distribution with the geometrical organization of modern clusters of seep sites. This lack of connection between isolated seep sites can be due to (1) poor outcrop conditions or stratigraphic uncertainty (Natalicchio *et al.* 2015) or (2) the large size of modern pockmarks, which are several hundred metres in diameter and only a few metres in depth (typically 500–800 m wide and 5–80 m deep), leading to difficult or incorrect correlations in the field (Gay 2002; Stewart 2015). To date, a fossil giant pockmark has never been identified nor characterized at outcrop, although some microbial assemblages have been reinterpreted in the light of examination of modern hot vents at mid-ocean ridges and cold seeps at continental margins (Whiticar 1999; Gay *et al.* 2006). This is the case for the fossil seep sites in the Jurassic limestones of Beauvoisin in the SE Basin of France, which were first interpreted as hydrothermal vents (Lemoine *et al.* 1982; Rolin 1987; Gaillard *et al.* 1996) and then
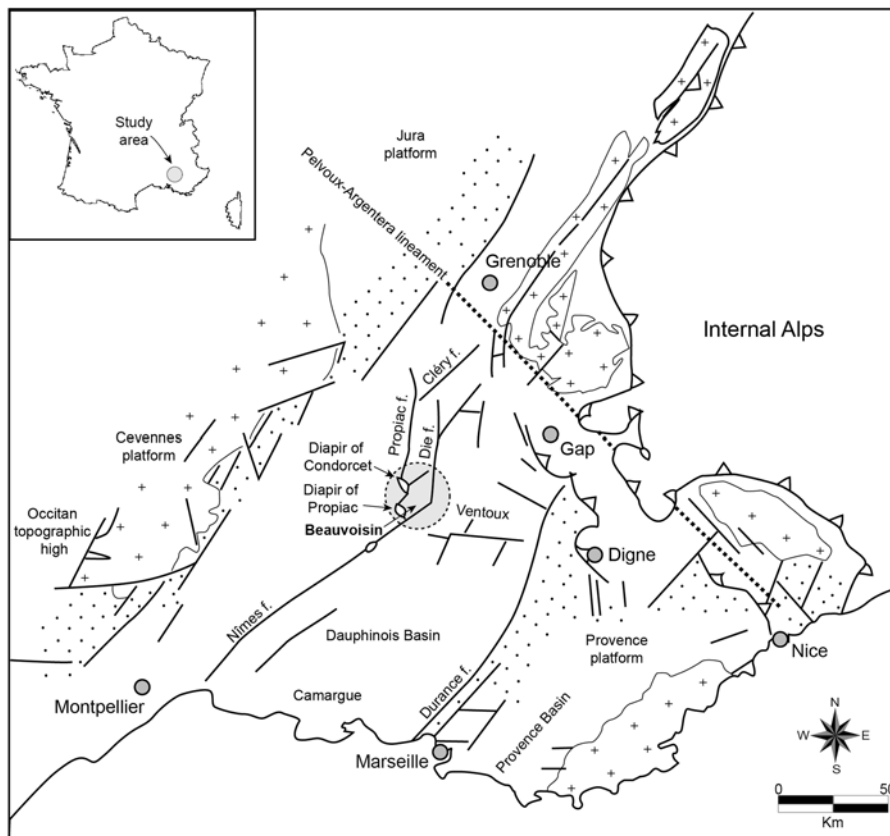
Fig. 1. Simplified structural map of the SE Basin of France. The study area is located south of the Pelvoux-Argentera lineament (external Alps, dotted line; cross symbols, igneous rocks) between the Propiac Fault and the Die Fault north of the Ventoux in a relay zone corresponding to the heritage of synsedimentary faults that structured the Jurassic Tethyan margin. In the Beauvoisin area (grey circle) the identified seep sites developed in dark marls called the 'Terres Noires' Formation (Oxfordian).

reinterpreted as cold seeps (Peckmann *et al.* 1999; Kiel 2013). The Beauvoisin seep site is of high importance as it is one of the few worldwide examples that is equivalent to Cenozoic chemosymbiotic-related fossil sites (Campbell & Bottjer 1995a; Louis-Schmid *et al.* 2007). All seep sites have generally been studied individually without consideration of any link to neighbouring sites, even those situated in more distant locations (Louis-Schmid *et al.* 2007). Furthermore, in the fossil record isolated carbonate lenses or groups of small-scale carbonate lenses, about 10 m wide and 5 m high, have often been considered as individual pockmarks or as a field of pockmarks respectively (Agirrezabala *et al.* 2013).

The aim of this paper is to characterize the 3D architecture of an 800 m wide cluster of fossil seep sites at Beauvoisin in the SE Basin of France, in the vicinity of Buis les Baronnies and Propiac (Drôme) (Fig. 1), based on the correlation of detailed sedimentological logs, sampling of key seep features such as carbonate lenses, marls and nodules, and related petrographical and geochemical analyses. The Beauvoisin architecture is then compared with that of the Regab giant pockmark in the Lower Congo Basin and with sandbox models simulating fluid injection at the base of a box filled with a matrix of water-saturated grains.

Methods and data

Since the first studies of the Beauvoisin site conducted in the 1980s (Gaillard *et al.* 1985; Rolin 1987; Rolin *et al.* 1990), recent erosion has exposed new sites, and to date 19 embedded carbonate masses (sub-sites A–T; see Fig. 2 for location) have been identified at various positions in the stratigraphic record, using the initial nomenclature of Rolin (1987). This suggests that all sites are not cropping out owing to vegetal cover and agricultural fields and some sub-sites are probably still to be found. To define precisely the stratigraphical relationship between the encasing fine-grained marls and the fossil-rich carbonate units, 23 stratigraphical logs were obtained through the entire area using a Jacob's stick, between 2002

and 2016. The precision is about 2 cm for each log. Field analysis of the Beauvoisin unit comprises identification of major stratigraphic and sedimentological features. The general correlation is related to the Tethyan sequences (Gradstein 2012) and some key layers were easily identified (Fig. 3), such as the few centimetre-thick bentonite layers documented by Pellenard *et al.* (2003), or the sub-continuous 10 cm to 1 m thick massive carbonate layers R1–R20 of the Argovian sequence identified by Gaillard *et al.* (1992). This study is based on the analysis of the macroscopic fabric of carbonate lenses related to the reference layers in the surrounding marls of the 'Terres Noires' Formation. Sampling for petrographical, mineralogical and geochemical analyses of the carbonate deposits was carried out on steep slopes in marls. Where thalwegs were not accessible for sampling or mapping, a drone was used for high-resolution photography. The obtained mosaics were coupled to aerial photographs and then georeferenced to topographic maps (IGN map #3140ET) to establish the areal distribution of outcrop (Fig. 2).

Analyses were conducted at the University of Barcelona for C and O isotopes. Forty-eight microsamples were prepared after the petrographic study to determine the carbon and oxygen stable isotope ratio of the different cements using the standard technique of Craig & Gordon (1965) and Claypool *et al.* (1980). The CO_2 was extracted from 60 ± 10 µg of powdered carbonate samples, which were reacted with 103% phosphoric acid for 2 min at 70°C for calcites. The CO_2 was analysed using an automated Kiel Carbonate Device attached to a Thermo Electron (Finnigan) MAT-252 thermal ionization mass spectrometer. The results are precise to ±0.02‰ for $\delta^{13}C$ and ±0.04‰ for $\delta^{18}O$.

The general organization of the fossil seep sites of Beauvoisin was then compared with the modern and active Regab pockmark in the Lower Congo Basin (Gay 2002; Ondreas *et al.* 2005; Gay *et al.* 2006; Marcon *et al.* 2014). Bathymetry and imaging data were acquired during various surveys between 1999 (ZAIANGO) and 2011 (WACS) using IFREMER's remotely operated vehicle (ROV) *Victor 6000*. The first survey was conducted during a site
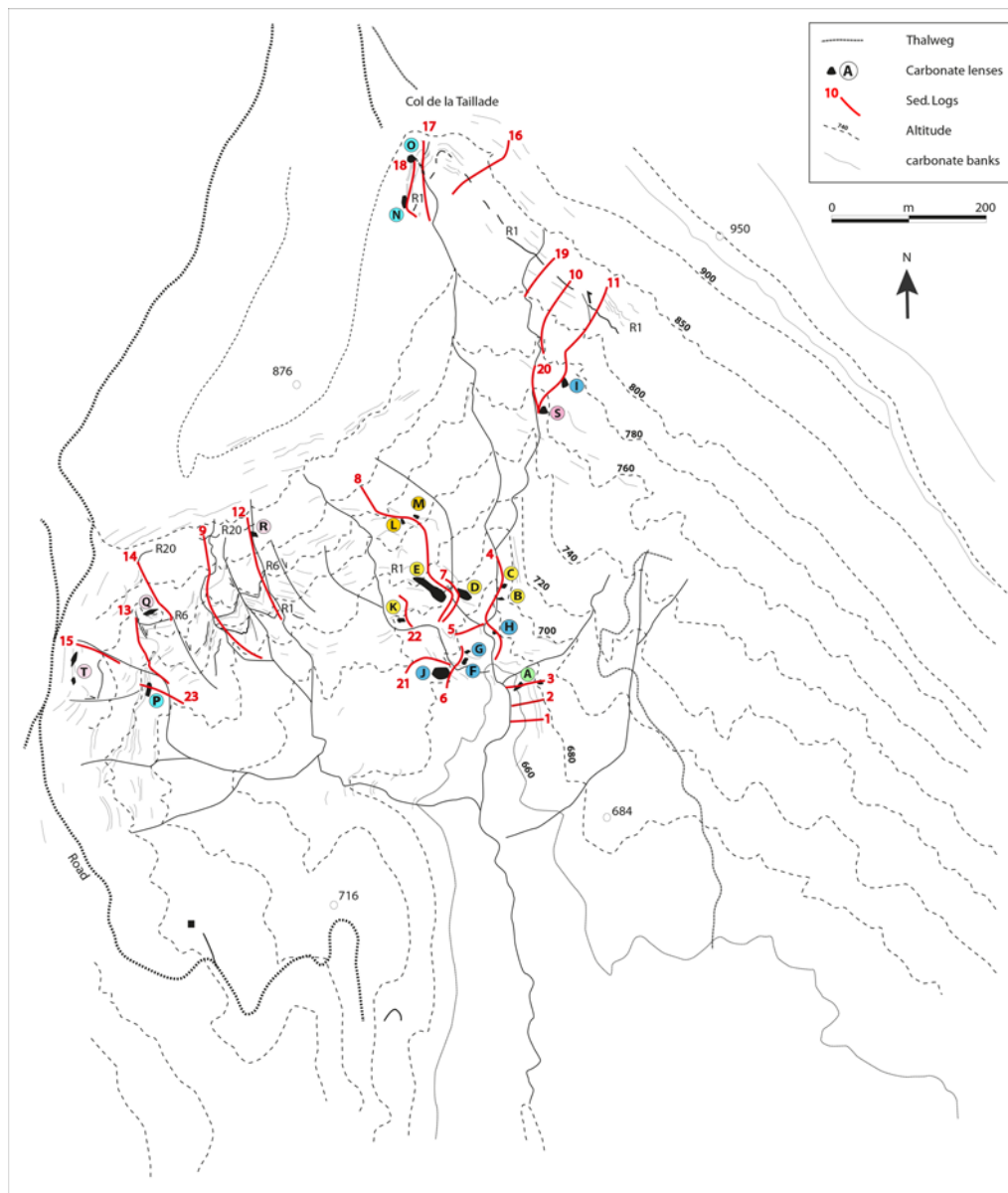
Fig. 2. Detailed topographic map of the Beauvoisin area (modified after Gaillard *et al.* 1985). Twenty-three sedimentological logs have been recovered (red lines) between 2002 and 2016 in steep valleys. Almost all valleys have been explored, depending on safety conditions. Nineteen sub-sites have been reported, including two new sites, S and T, that were exposed as a result of weathering since the initial mapping.

exploration and mosaicking at about 2 m above the sea-bottom. The main survey was then conducted from 30 m above the seafloor using a Reson Seabat 7125 multibeam echosounder (MBES) running at 400 kHz.

The sandbox model consists of a Plexiglas cylindrical tank (24 cm diameter) for the 3D and a vertical Hele–Shaw cell (glass plates 40 × 30 cm, separated by a 2 mm gap) for the 2D laboratory experiments. Both systems are filled with particles immersed in water and a constant flow of air, Φ, is injected from a single inlet centred at the base of the cell. The particles are polydispersed, spherical glass beads (Sovitech glass spheres), sieved to obtain four batches with particle diameters $d = 218 \pm 17$, 318 ± 44, 631 ± 37 and 802 ± 68 µm. The grain-size distribution for the different batches is measured by means of a microscope (Optika B-163) and roughly displays a Gaussian shape (Ramos *et al.* 2015). In the 2D experiment the grain dynamics are tracked by analysing the absolute difference in the intensity of two consecutive images, which gives access to regions where motion occurred in the immersed granular layer owing to the ascending gas flow. To quantify the generation of the fluidized zone, which corresponds to a cumulative process

owing to the continuous gas emission, we define the normalized flow density, computed as the cumulation of successive image differences (Ramos *et al.* 2015; Varas *et al.* 2015; Poryles *et al.* 2016). This variable makes it possible to quantify the regions where motion occurred (disturbed particles).

Geological setting

The Beauvoisin seep site is located in the northern part of the SE Basin of France (Fig. 1), which is related to the Jurassic opening of the Liguro-Tethyan Ocean (Lemoine 1985). From the Hettangian to the Bathonian the basin was a shallow-water carbonate platform with frequent subaerial exposure or erosion indicating a stable margin with a low rate of subsidence. From the Bathonian, sedimentation compensated for the moderate subsidence of the southern platform and environments remained shallow, whereas along the northern platform cherts and organic-rich marls indicate a general deepening of at least 600 m (Dardeau 1988). From the Oxfordian, general subsidence affected the entire platform, moderate in the southern part (reefal facies and confined
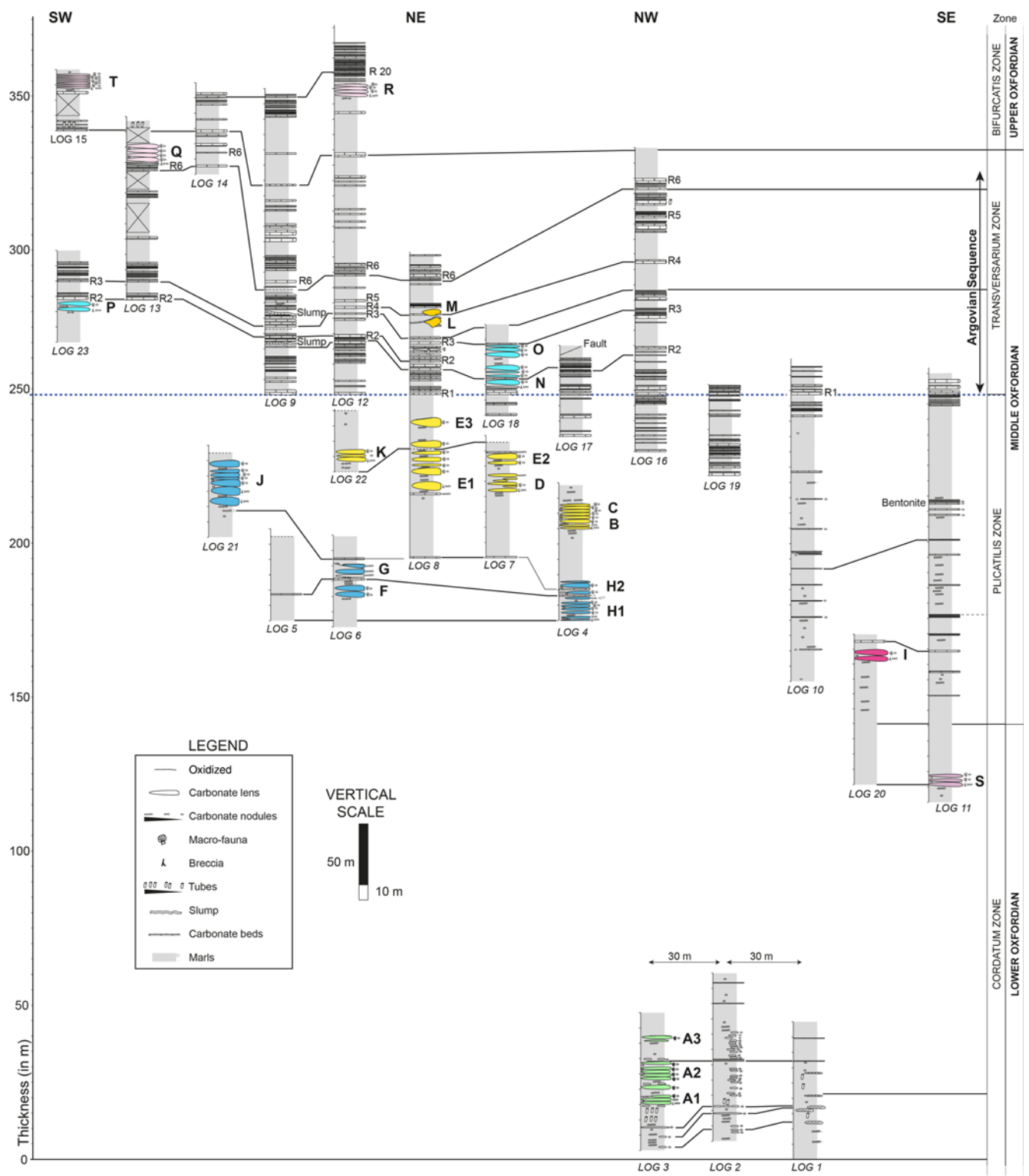
Fig. 3. Correlation of the 23 sedimentological logs in the Beauvoisin area regarding the general stratigraphy of the Oxfordian. The 23 stratigraphical logs were obtained utilizing key marker layers, R1–R20, following the nomenclature of Gaillard *et al.* (1985) and Rolin (1987). The correlation is centred and flattened on the R1 level corresponding to the base of the Argovian sequence ending on top with the R6 level.

environments) and increasing in the northern part (deep marl facies and submarine slides).

In the Beauvoisin area the identified seep sites occur in the deepest, central part of the basin where the subsidence was at a maximum from the Bathonian to the Oxfordian (Gaillard *et al.* 1985). This led to deposition of up to 2000–2500 m of organic-rich marls called the 'Terres Noires' Formation, limited to the north by the Jura high, to the west by the Cevennes domain and to the east by

the Briançonnais domain of the Western Alps (Fig. 1). The 'Terres Noires' Formation has also been identified in boreholes in the south in Camargue and Provence (Dardeau 1988). Subsidence was mostly due to basement faults with kinematics controlled by salt withdrawal in the extensional domain of the margin (Mascle 1988). The fluid seep sites are bounded to the west by major salt-rooted faults, which facilitated growth of the main salt diapirs into the marls, as at Propiac and Condorcet (Fig. 1).

The 'Terres Noires' Formation is divided into three main intervals corresponding to the three major geodynamical episodes that affected the margin (Gaillard *et al.* 1985; Rolin 1987; Gaillard & Rolin 1988; Rolin *et al.* 1990). The Bathonian sequence is characterized by marls alternating with thin mudstone layers. The Callovian to Middle Oxfordian sequence is dominated in the lower part by centimetre- to multi-centimetre-thick dolomudstones and in the middle and upper part by marls containing isolated red to grey nodules ('Nodules Chocolat' of Artru 1972). The upper Oxfordian is composed of marls alternating with multi-centimetre- to metre-thick dolomudstone layers in a general thickening upward sequence. The transition to the Kimmeridgian is marked by the Argovian sequence composed of thick amber dolomudstone layers alternating with light brown marls.

Dating the origin of focused fluids has never been clearly elucidated. They have been hypothetically related to crustal faults (Lemoine 1985), to halokinesis (Mascle 1988) or to a biogenic origin derived from the decomposition of organic matter contained in the 'Terres Noires' Formation (Gaillard *et al.* 1996). Fluorescence microscopy on fluid inclusions coupled to stable carbon isotope analyses has shown the presence of oil containing *n*-alkanes generated from thermal maturation of organic matter from the sedimentary pile (Peckmann *et al.* 1999). The latter is consistent with the total thickness of the 'Terres Noires' Formation, which has clearly reached a burial depth through the oil window in the lower part.

Log correlations

The fossil-rich carbonate suite of Beauvoisin crops out within the thick succession of well-stratified Jurassic marls of the 'Terres Noires' Formation in the Lower to Upper Oxfordian interval (Gaillard *et al.* 1985). Between 2002 and 2016, 23 stratigraphical logs were collected, allowing a detailed correlation of the 19 sites (A–T) related to the general stratigraphy of the Oxfordian marls (Fig. 2). All sites are concentrated west of Beauvoisin and south of the 'Col de la Taillade' (Fig. 2) where they are exposed in very steep valleys between 660 and 870 m altitude. This work is based on the initial nomenclature established by Gaillard *et al.* (1985) and Rolin (1987). They grouped together carbonate lenses in sites from A to R (Rolin *et al.* 1990). The intense weathering in spring and autumn in the region for the last 30 years has allowed two new sites to be exposed in the Terres Noires Formation. The sites S and T were integrated into the general stratigraphy of Beauvoisin in logs 11 and 15, respectively (Fig. 2).

The 23 stratigraphical logs were constrained using key layers, R1–R20, following the nomenclature of Gaillard *et al.* (1985) and Rolin (1987). However, additional layers (not displayed in this study) were also used following Gaidon *et al.* (1988) and Pellenard *et al.* (1999, 2003). This included the identification of a bentonite layer, located at about 220 m above the bottom of log 1 (Fig. 3), which is the reference for all measurements in this study. Some centimetre-thick ochre and gypsum-rich layers were also recognized in the area. They can be correlated over all the basin and mark some regional events (Pellenard *et al.* 1999). The correlation is centred and flattened on the R1 level corresponding to the base of the Argovian sequence ending on top with the R6 level. It is characteristic of the upper part of the Oxfordian in the SE Basin of France and it is composed of decimetre- to metre-thick, yellowish to light brown limestones alternating with light grey marls and claystones.

It is worth noting that the thicknesses of the Argovian sequence vary by a factor of 3–4 over a distance of 700 m, which is the longest distance between two logs in the area. For instance, this is the case for the R2–R6 interval, which is about 110 m thick in log 16 (north), 60 m thick in log 8 (centre of the area), 30 m thick in log 9 (west) and 90 m thick in log 13 (SW) (see Fig. 2 for location). In particular, log 9 shows evidence of intense deformations owing to slumps at

260 and 275 m (Fig. 3). The thickness variations in the Argovian sequence could be due to syn- to post-depositional erosion or slump processes, which increase towards the centre of the area.

Based on the log correlation it is then possible to generate a composite log taking into account the eroded missing sequences, slump deposits and faults (Fig. 4). When varying laterally, the thickest part of a sequence was kept, to correspond to the 360 m total thickness of the studied Oxfordian interval. On this composite log, the oldest site A is located within the *Cordatum* Zone (Lower Oxfordian) whereas the youngest site T is in the *Bifurcatis* Zone (Upper Oxfordian). Given the uncertainty of absolute dating in the Jurassic, the Tethyan sequences and age model from Gradstein (2012) are reported on the right side as an indication only. The figure shows that only two sites (A and S) developed in the *Cordatum* Zone, corresponding to the Lower Oxfordian, whereas most sites developed in the *Plicatilis* Zone (B, C, D, E, F, G, H, I, J, K) and in the *Transversarium* Zone (L, M, N, O, P, Q), which are Middle Oxfordian in age, and only two sites (R and T) developed in the *Bifurcatis* Zone, corresponding to the Upper Oxfordian (Fig. 4). Given an average rate of sedimentation and a constant compaction rate within the interval, 310 m were deposited in 3.1 myr between 157.4 and 160.5 Ma. The base of site A1 at 15 m and the top of site T at 359 m can be estimated at 157.14 Ma and 160.58 Ma respectively as a first approximation. Despite 15 years of fieldwork in the area, no more sites have been discovered beneath site A or above site T. However, this does not mean that they do not exist as they may have not been exposed yet, like the newly discovered sites S and T. To date, sites A–T can be estimated to occupy a duration of a total of 3.44 myr with an average rate of 10 cm per 1000 years of sedimentation.

Vertical organization of seep facies

The 19 sites A–T correspond to carbonate lenses encased in marls or claystones and forming local unconformities in the Terres Noires Formation. Each site taken individually is organized as subvertically stacked, 2–15 m wide, lenses that are in contact (i.e. the top of an underlying lens is in sharp contact with the bottom of the overlying lens) or interbedded with marls. For sub-site F (Fig. 5a), the three basal carbonate lenses, 1–1.5 m thick and 5 m wide, are in contact with each other and the two top carbonate lenses, 0.5–1 m thick and 3 m wide, are interlayered with a 0.8–1 m thick interval of nodule-rich marls. Sub-site F forms a 7 m high edifice composed of subvertically stacked carbonate lenses, lenticular in shape. The two first basal lenses are brecciated showing various-sized, cemented, sub-angular clasts (Fig. 5b). In detail, two major types of breccia were identified: (1) a matrix-supported cemented macro-breccia made up of centimetre- to decimetre-sized sub-angular and microsparite clasts within a yellowish or light brown microbial carbonate matrix; (2) a dark brown cement-supported micro-breccia made up of millimetre- to multi-millimetre-sized clasts within a slightly oil- or bitumen-impregnated matrix.

This brecciated facies is in close association with subvertical mineralized veins (Fig. 5b). The veins are filled by several generations of carbonate cement. The first generation is an iron-rich drusy calcite, 20–300 mm thick, followed by bladed, high Mg-calcite or aragonite and then by 550 mm of botryoidal aragonite forming the final cement generation (Peckmann *et al.* 1999). The matrix-supported cemented macro-breccia comprises clasts, the shape of which is concordant with the massive matrix of the carbonate lenses, suggesting a jigsaw puzzle-like structure (Fig. 5b and c). The dark brown cement-supported micro-breccia is more concentrated towards the veins and at some places surrounding the mineralization.

The carbonate lenses are dominated by mollusc macrofossils mostly represented by lucinid bivalves *Beauvoisina carinata* (Gaillard *et al.* 1985, 1992; Rolin *et al.* 1990), gastropods including
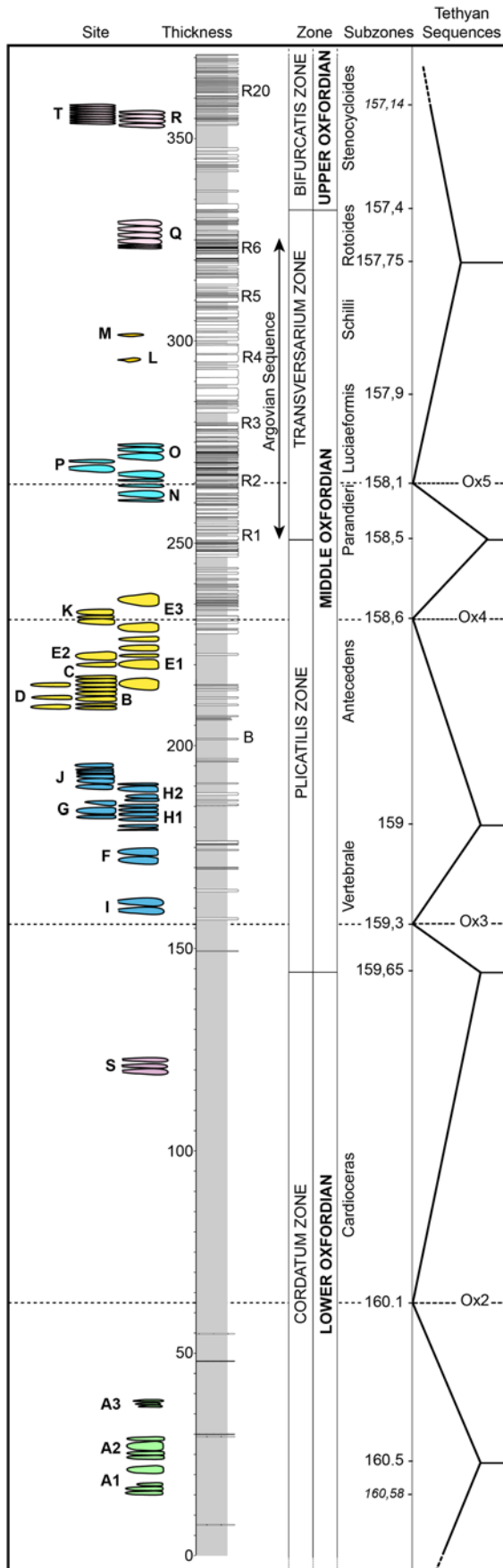
Fig. 4. Composite log of the Oxfordian in the Beauvoisin area taking into account eroded missing sequences, slump deposits and faults (360 m in thickness). The oldest site A is located within the *Cordatum* Zone (Lower Oxfordian) whereas the youngest site T is in the *Bifurcatis* Zone (Upper Oxfordian) according to the Tethyan sequences and age model from Gradstein (2012).

Paskentana umbilicata, *Hokkaidoconcha novacula* (Kiel 2013) and cephalopods such as ammonites (Rolin *et al.* 1990). Lucinids are usually restricted to carbonate lenses and they are not found in surrounding marls, suggesting that they were endofauna. They can form dense groups with some lucinid specimens reaching 18 cm in diameter (Rolin 1987). The shells provide average positive δ^{13}C values as high as +5‰ PDB (Pee Dee belemnite; Peckmann *et al.* 1999), probably owing to symbiosis with chemosynthetic bacteria (Rolin *et al.* 1990; Gaillard *et al.* 1992). However, the δ^{13}C values range between −26.5 and +13‰ PDB in carbonate lenses (Peckmann *et al.* 1999), which is consistent with the more recent values measured at site F by Tribovillard *et al.* (2013) (−18.8‰ < δ^{13}C < +12.7‰ PDB). In the basal lenses of site F, some lucinid specimens, 12–15 cm wide, were observed very close to the brecciated facies and mineralized veins (Fig. 5c). Some other species have been identified, such as crustacean exoskeletons, fragments and coprolites, belonging to the form-genus *Favreina* and attributed to the anomuran superfamilies Thalassinoidea and Galatheoidea, as well as fish teeth (reflecting the presence of additional predators or scavengers), sponge spicules and the irregular echinoid *Tithonia oxfordiana* (Gaillard *et al.* 1985, 1992, 2011; Senowbari-Daryan *et al.* 2007; Kiel 2010). Probable deposit feeders, such as holothuroids (*Sclerites*), and suspension feeders, such as crinoids (ossicles), are found in minor abundance (Gaillard *et al.* 2011). Benthic foraminifers (such as Spirillinidae, Nodosariidae, Textulariidae and *Ophthalmidium*), ostracods, planktonic foraminifers (proto-globigerinids), radiolarians and dinoflagellates are present but less numerous. Sponges are also frequent, mainly lyssacid hexactinellids, accompanied by lithistid demosponges, unidentified demosponges and lychniscid hexactinellids (Gaillard *et al.* 2011). These biota are common in the Jurassic seafloor in the area, suggesting a bathyal environment estimated around 600 m water depth (Tribovillard *et al* 2013). Ovoid to irregularly shaped fecal pellet concentrations locally scattered in the micrite indicate benthic activity (Gaillard *et al.* 1985, 1992, 2011).

The Oxfordian seep carbonates are very rich in micritic nodules, millimetres to 15 cm in diameter depending on their position relative to carbonate lenses (Fig. 5d). These concretions formed around body fossils, such as ammonites, bivalves, spicules and any biodetritus or burrows (Gaillard *et al.* 1985; Rolin 1987). Nodules are darker than the micritic matrix and are densely packed within the basal carbonate lenses, where they form millimetre to 2 cm aggregates encased in a dark micrite (Fig. 6a). They contain framboidal pyrite, 40–250 mm in diameter, and are often lined by an outer rim of pyrite (Peckmann *et al.* 1999; Gay 2002). The δ^{13}C values in nodules range between −26.5 and −22.8‰ PDB (Peckmann *et al.* 1999), with minimum values similar to the encasing carbonate lenses. They become scattered towards the margins and they can form 5–10 cm long twin nodules where the carbonate lenses thin (Fig. 6b). Twin nodules are separated from each other over a distance between a few decimetres to about 1 m. These nodules appear at the same stratigraphical level as 15 cm nodules separated from each other by a few decimetres to a few metres (Fig. 6b). Other small nodules, 15 cm to millimetres in diameter, can be found at the same stratigraphical level over a distance of 30–60 m from the centre of the carbonate lens (Fig. 6b). However, their diameter decreases as the distance to each other increases with distance from the carbonate lens. Beyond 60 m from the carbonate lens, they completely disappear. Bitumen is frequent within the nodules encased in marls but not in nodules encased in carbonate lenses. Other types of concretions related to sponge taphonomy and burrowing were locally described by Gaillard *et al.* (2011).

The carbonate lenses are composed of a micritic matrix rich in Mg-calcite, aragonite and dolomite, which are the common authigenic minerals at cold seeps (Roberts *et al.* 1993). Previous
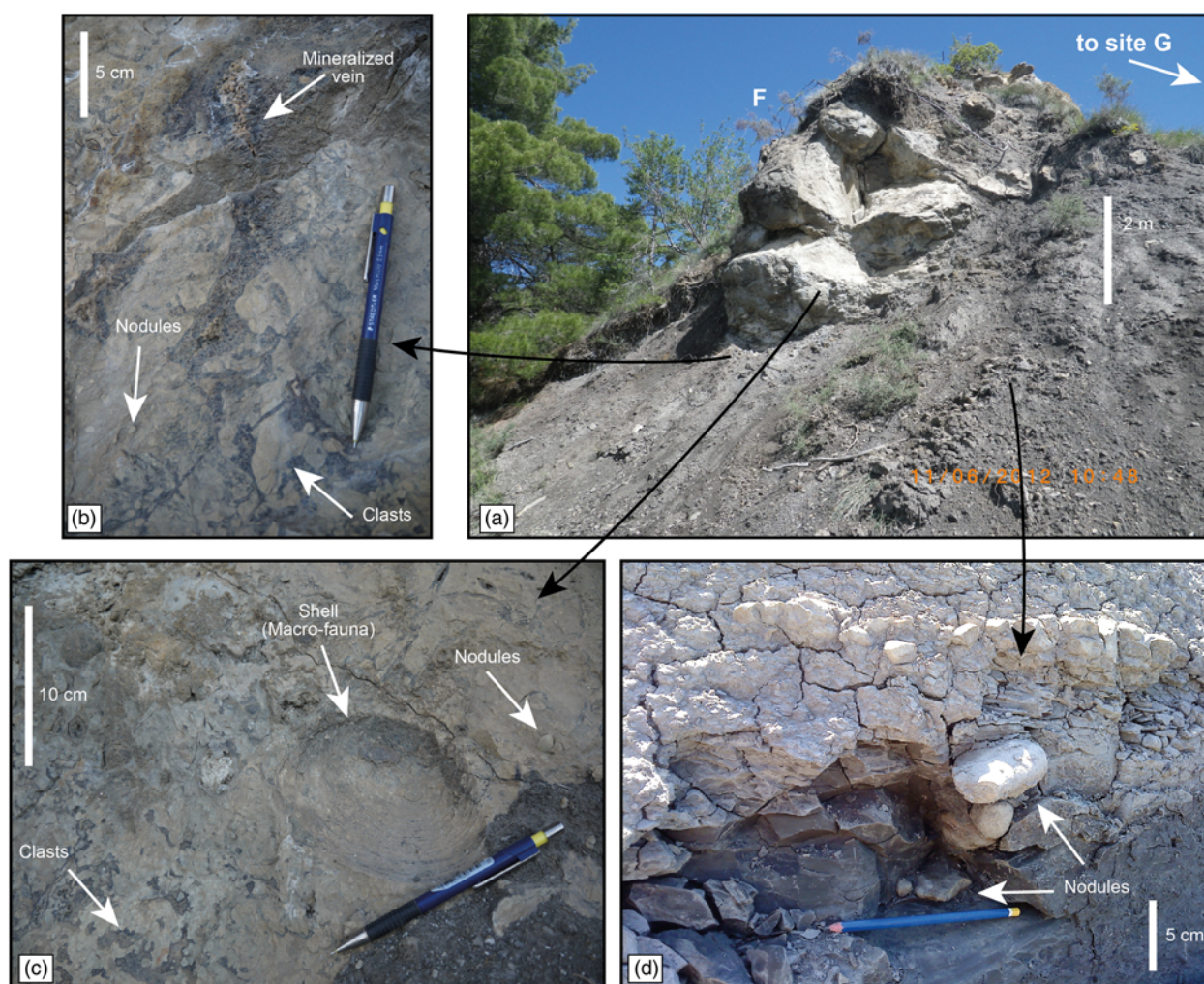
Fig. 5. Sub-site F located in the centre of the Beauvoisin area (see Fig. 2 for location). (**a**) View to the west of site F forming a 7 m high edifice composed of subvertically stacked carbonate lenses. (**b**) Detailed photograph of the basal carbonate lens showing the brecciated facies dominated by subvertical veins yielding mineralizations and displaying a jigsaw puzzle-like structure. (**c**) Detailed photograph showing lucinid specimen, 12–15 cm wide, in close association with the brecciated facies and mineralized veins. (**d**) Detailed photograph showing micritic nodules, millimetres to 15 cm in diameter.

analyses conducted on marls show $\delta^{13}C$ values ranging between −19 and −17.7‰ far from the carbonate lenses (Peckmann *et al.* 1999). These values increase close to the carbonate lenses (−0.7‰ < $\delta^{13}C$ < +1.1‰), as was also reported by Tribovillard *et al.* (2013). In addition, different types of carbonate cements were identified, such as splayed calcite, yellow calcite and botryoidal aragonite and calcite (Beauchamp & Savard 1992). In particular, the botryoidal fabric is presumed to be of bacterial origin (Roberts *et al.* 1993), with values of $\delta^{13}C$ between −14.8 and −12‰ (Peckmann *et al.* 1999), reinforcing the role of microbial mediation in the building of carbonate lenses.

The top of the upper lens of many sub-sites is affected by pervasive corrosion creating vugs and irregular surfaces. For instance, on top of sub-site G (see Fig. 2 for location), the corrosion formed a multi-centimetre-thick Mn- and Fe-rich crust (Fig. 6c), which is often associated with pyrite. Remnant pyrite-encrusted micrite nodules can be found in overlying marls for a few centimetres to a few decimetres above the oxidized crust (Fig. 6d).

Seeping sub-sites

The sub-site A is one of the more recognizable sub-seep sites of the Beauvoisin area (see Fig. 2 for location). It was first described as a columnar structure, different from other sub-sites B–T considered as lenticular (Gaillard *et al.* 1985; Rolin 1987). However, the outcrop conditions with steep flanks of the Terres Noires did not give access to sub-site A until we used climbing ropes and harnesses. Sub-site A is composed of lenticular carbonate lenses that are currently intensively eroded by present-day weathering (Fig. 7). All carbonate lenses that are in sharp contact with each other are considered as one unit. In consequence, three main units can be defined, forming, from base to top, sub-sites A1, A2 and A3. In terms of stratigraphic position, sub-sites A1–A3 are Early Oxfordian in age (see Fig. 3 for the log correlation), belonging to the *Cordatum* Zone at about 160.5 Ma (see Fig. 4 for age estimation). Three high-resolution stratigraphic sections were obtained in the area. Logs 1 and 2 are located respectively 60 and 30 m SE of the sub-sites A1–A3, whereas log 3 follows the crest descending through the three sub-sites A1–A3 (Fig. 7). At this scale, relevant levels 1–5 can be visually correlated from log to log following the general stratigraphy (S_0). Levels 1–4 correspond to aligned nodules following the general stratigraphy whereas level 5 is a multi-centimetre-thick layer of mudstone. All sections were flattened on level 5 located on top of sub-site A2 in log 3 (Fig. 8). The first remarkable feature is that all levels are at the same topographic level in logs 1 and 2, but levels 1–3 are located 4–6 m beneath the general stratigraphy at the base of log 3. Despite our efforts, level 4 cannot be identified in log 3 directly beneath sub-site A1. All levels, including the flat level 5, are marked by a decrease in nodule concentrations from log 3 to log 1. The number of nodules per volume of marls is markedly reduced
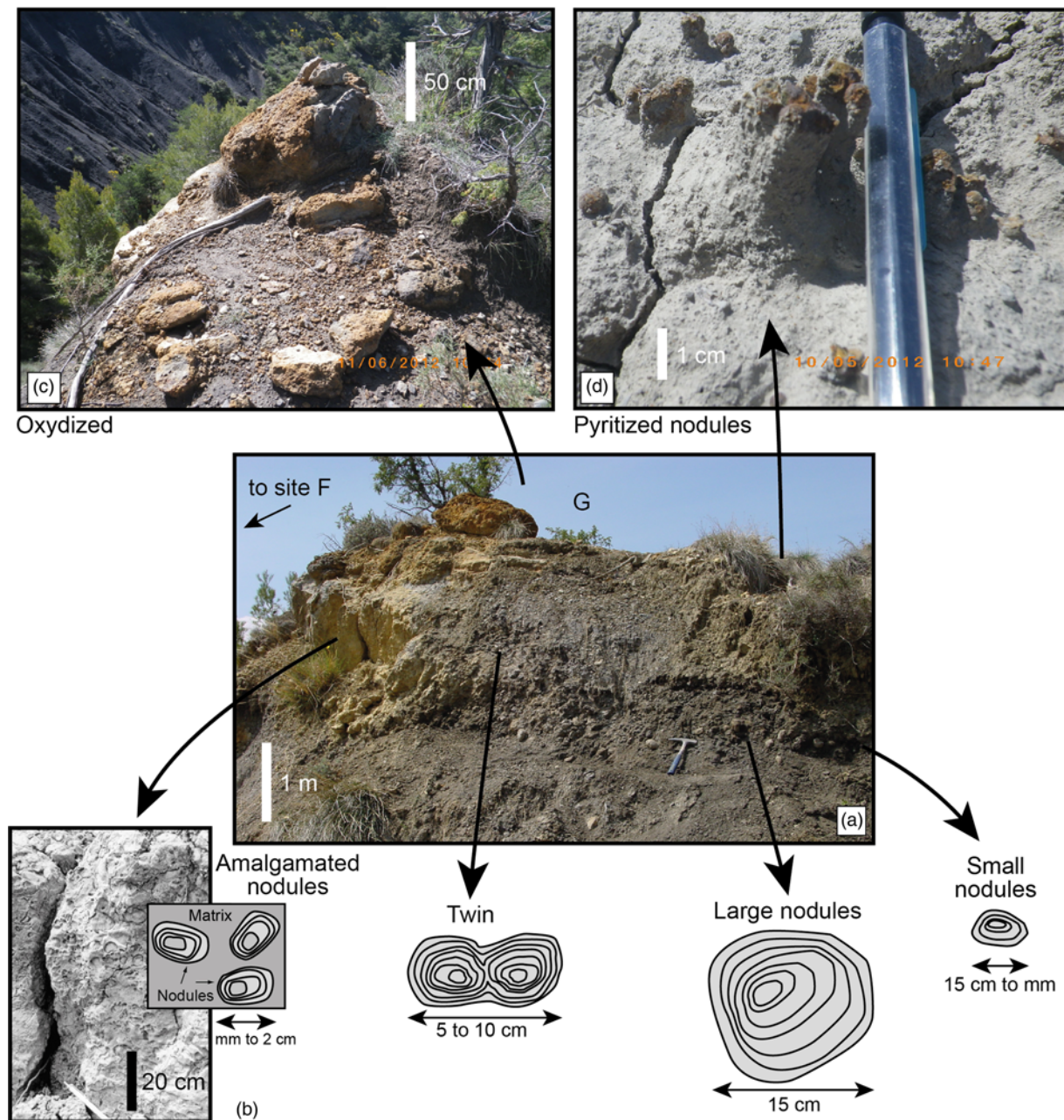
A. Gay *et al.*

Fig. 6. Sub-site G located in the centre of the Beauvoisin area and just above sub-site F (see Fig. 2 for location). (**a**) Outcrop photograph showing densely packed millimetre to 2 cm aggregates nodules encased in a dark micrite within the basal carbonate lenses. (**b**) Organization and shape of nodules depending on their distance to the carbonate lens. (**c**) Photograph of the top of sub-site G showing corrosion forming a multi-centimetre-thick Mn- and Fe-rich crust. (**d**) Detailed photograph showing pyrite-encrusted micrite nodules overlying marls for a few centimetres to a few decimetres above the oxidized crust.

beyond log 1 (i.e. beyond 60 m) and the nodules almost fully disappear beyond 70–80 m; for example, at Site G (see Fig. 6).

Comparison with an active seep site

Sub-seeps were previously identified at the bottom of the Regab giant pockmark in the Lower Congo Basin, where an 800 m wide and 15 m deep depression at about 3150 m water depth has been documented (Gay 2002; Ondreas *et al.* 2005). The average slope is about 2–3° compared with the surrounding seafloor. The detailed microbathymetry was obtained onboard the ROV *Victor 6000* during the ZAIROV 2 and BIOZAIRE cruises in 1999–2000. The first observations show that the giant pockmark is composed of several depressions, each about 100 m wide and 6 m deep (Ondreas *et al.* 2005). In detail, the small-scale depressions are not homogeneously distributed at the bottom of the pockmarks

(Fig. 9a). The deepest two depressions are located near the centre of the Regab pockmark field. They are marked by steep flanks with an angle of about 5° compared with the horizontal plane, locally reaching 7° if compared with the regional slope whereas other small-scale depressions have smoother slopes with an angle of about 1–2° (Fig. 9b). They all have a flat bottom, meaning that they look more like a plate than a bowl structure. This is consistent with the spider structures identified at shallower depths in the Lower Congo Basin (Casenave *et al.* 2017). However, only a few concretionary carbonates have been recovered in gravity cores from the Regab giant pockmark field (Gay *et al.* 2006). This apparent lack of nodules or concretions may be due to the inability of modern coring techniques to adequately sample such carbonates (Loyd & Berelson 2015).

The studies conducted in the Regab pockmark field have shown that the highest concentrations of methane (up to $150\,\mu l\,l^{-1}$) in bottom waters were measured near the centre of the main
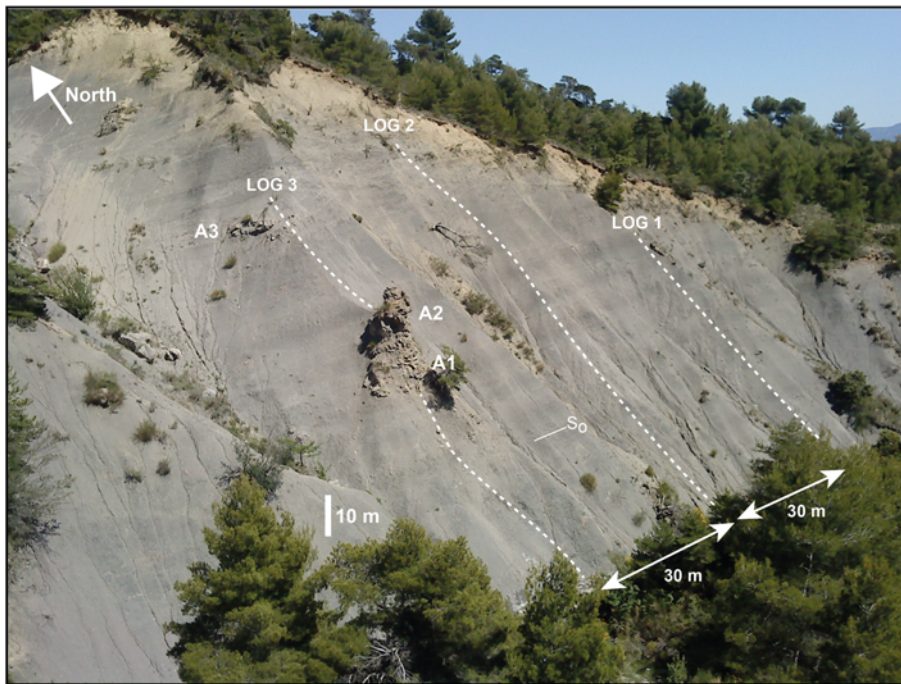
Fig. 7. Photograph to the NE taken from site G and showing site A in the Lower Oxfordian (see Fig. 2 for location). Three sub-sites, A1–A3, can be identified from the base to the top. Three high-resolution stratigraphic sections, logs 1–3, were obtained at 60, 30 and 0 m (vertical axis of the three sub-sites A1–A3).

depression, suggesting that this area is the actual and active methane seepage point (Gay *et al.* 2006). More precisely, a recent study showed that only two zones are actually harbouring tubeworms, mussels and clams at the same time, all living in close association with 4 m high carbonate build-ups (see fig. 2b of Marcon *et al.* 2014), also a common feature of other giant structures such as in the Hydrate Ridge (Teichert *et al.* 2005) and in the Mediterranean Sea (Ingrassia *et al.* 2015). These two zones are annotated with green arrows in Figure 9b and they correspond to the two deepest small-scale depressions identified on the dip map of the Regab pockmark field. In addition, sea-bottom pictures and videos taken within the

other small-scale depressions displayed only relict features such as carbonate pavement oxidized on top and surrounding dead fauna or fields of clams on reduced black sediments (red arrows in Fig. 9b). This may indicate a 'fossil' site as remnant methane seepage ($<20 \ \mu l \ l^{-1}$) in bottom waters coupled to dead or dying fauna and oxidized crusts, suggesting that fluid fluxes may have operated at higher rates in the past (Gay *et al.* 2006), as observed in other active and modern seep sites (Greinert *et al.* 2001; Han *et al.* 2004; Haas *et al.* 2010). This also suggests that only one or two points of focused fluid emission can act in a pockmark field, such as for the Hydrate Hole further north in the Lower Congo Basin (Wenau *et al.*
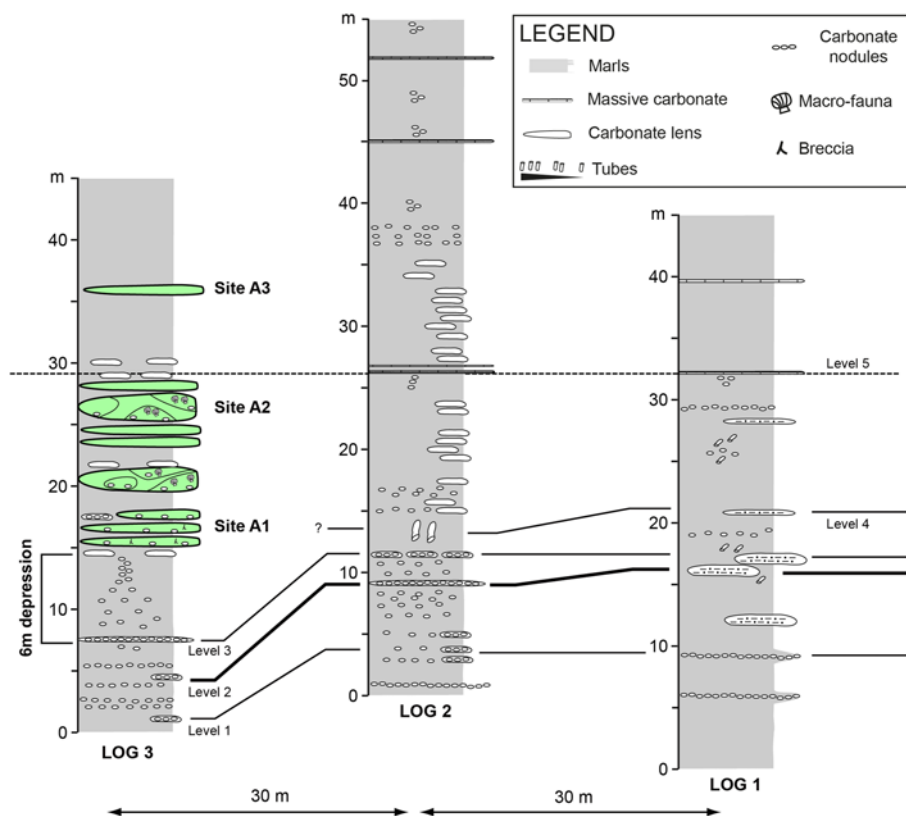

Fig. 8. Sedimentological logs 1–3 obtained at site A (see Fig. 2 for location; see Fig. 7 for the detailed location). All sections were flattened on level 5 located on top of sub-site A2 in log 3. Levels 1–3 are located 4–6 m beneath the general stratigraphy at the base of log 3, defining a smooth depression. All levels are marked by a decrease in nodule concentrations from log 3 to log 1.
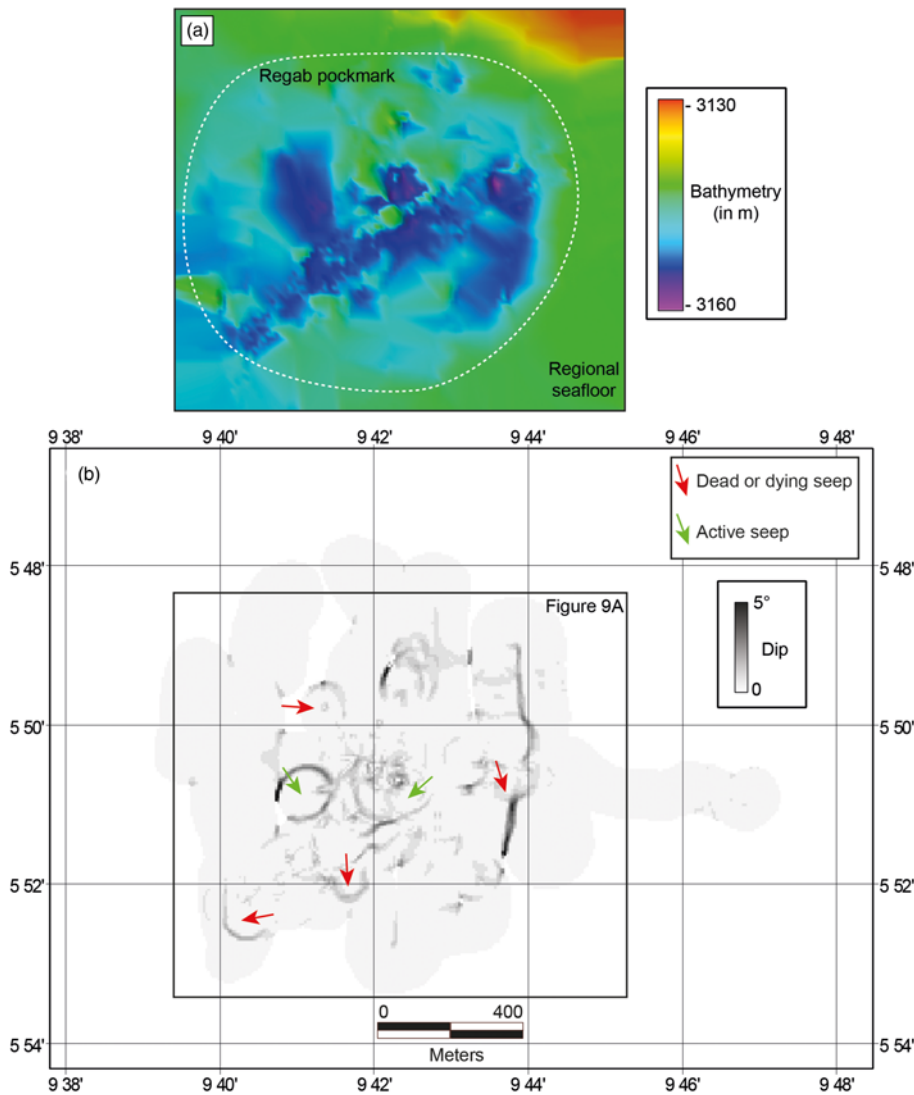
Fig. 9. (**a**) High-resolution bathymetric map of the Regab pockmark, acquired during the ZAIROV and BIOZAIRE scientific surveys in 2000–2002. (**b**) Dip map of the Regab pockmark derived from the bathymetric map. It shows well-expressed 100 m wide sub-circular depressions. Green arrows represent the depressions with active and high-concentration methane seepage corresponding to the most active area (Gay *et al.* 2006). Red arrows represent intermediate or low methane flow rates interpreted as dormant or dying sub-sites.

2017) and in other giant pockmark fields such as in the Zannnone area (Ingrassia *et al.* 2015). This is probably due to the pressure gradient allowing only one path at a time to be open, as in any plumbing system (Gay *et al.* 2007).

Clustering of fluid venting

Predicting the pattern of gas invasion and rise in liquid-saturated sediments is still a challenge. From a theoretical point of view, the relative importance of the dominant forces in the system (i.e. buoyancy and capillary forces) has to be taken into account. The Bond (or Eötvös) number, defined as the ratio of gravity to capillarity forces, is traditionally used to characterize multiphase flow in porous media. However, this number does not account for the different spatial scales that govern the dominant forces. Indeed, the largest capillary overpressure is controlled by the narrowest space between grains ('pore neck') whereas the largest buoyancy force is controlled by the wider pore space ('pore body'). To take into account this so-called porous media aspect ratio, a modified Bond number has been introduced by Brooks *et al.* (1999). This dimensionless parameter allows a physical classification of the flow patterns, which strongly depend on the porous media aspect ratio (Selker *et al.* 2007). This latter, however, is difficult to estimate, in particular in geological settings where porosity, permeability and grain distribution may drastically change over short distances.

Laboratory experiments were therefore developed to investigate gas invasion into liquid-saturated grains in polydispersed systems.

They bring the advantage of being closer to field situations while still allowing a precise control of the imposed parameters (geometry, grain-size distribution, injected gas flow-rate and so on). These sandbox models have been used to illustrate different regimes of gas invasion in the liquid-filled granular medium (see, for instance, Selker *et al.* 2007; Varas *et al.* 2015, and references therein): formation of gas channels, dendritic invasion, fracturing, etc. Sandbox experiments were recently conducted to investigate the temporal variations of gas emission owing to gas invasion into liquid-saturated grains (Vidal *et al.* 2010; Varas *et al.* 2011, 2015). In a 3D experiment (Fig. 10a), a constant air flow-rate (Q) is injected at the bottom of a layer of grains immersed in water. The gas is injected via a dry chamber (volume V), through a nozzle of inner diameter 1 mm, localized at the bottom centre of the cell (Fig. 10a). The pressure variations in the chamber are monitored with a pressure sensor. Surface imaging makes it possible to quantify the gas emission location and dynamics. The analysis of the position of bubble emissions shows that they can migrate laterally through time (Fig. 10b). Indeed, the distance from the centre (i.e. vertical axis of the injection point; red cross in Fig. 10b) varies from zero to a few centimetres in any direction of the cell, for an initial grain height h_g = 14 cm. No specific pattern appeared at this stage, probably because grain supply simulating sedimentation has not been implemented yet in the experiment. However, two stable states of gas emission were reported during the experiment. For a significant period of time, bubbles were expelled at roughly the same position, with a minor lateral migration, defining the clusters C1 and C2 at a
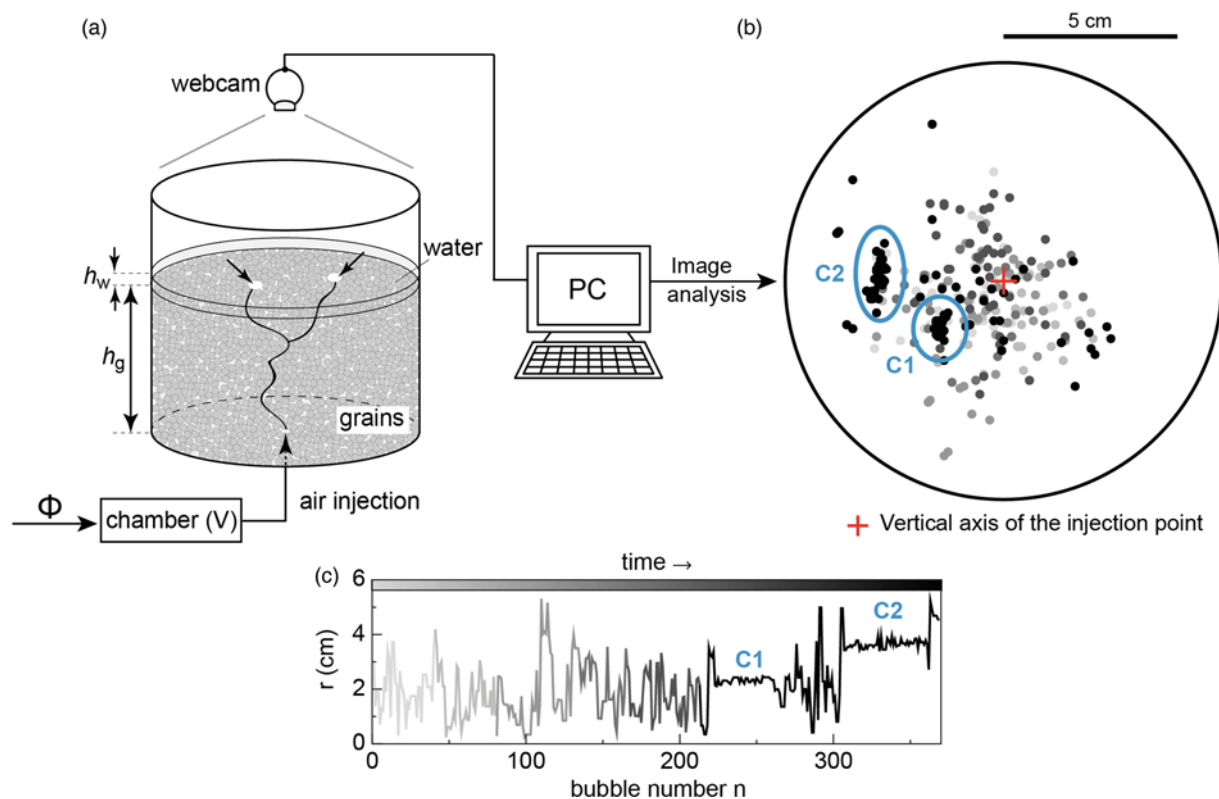
Fig. 10. Three-dimensional sandbox experiment (Varas *et al.* 2015). (**a**) Experimental setup. Air is injected at a constant flow rate Φ at the bottom of an immersed granular column (h_g is the height of grains and h_w the height of water above the granular bed). Bubble emission at the free surface is recorded by a webcam positioned over the experimental cell. (**b**) Detection of bubble emission at the free surface ($d = 318 \pm 44$ μm, $h_g = 14$ cm, $h_w = 2$ cm, $\Phi = 4.3$ ml s^{-1}; the colour of dots from light grey to black is proportional to time). The system releases bubbles in different (uncorrelated) positions. For two significant periods of time, however, several successive bubbles are emitted in a narrow region (clusters C1 and C2). This indicates the formation of a gas channel fixed at depth (region C1), which then collapses before it can reopen in another region (C2). (**c**) Distance r between the bubble emission location and the centre of the cell (red cross in (**b**)) as a function of the bubble number n for the sequence presented in (**b**).

distance of about 2.5 and 4 cm from the centre, respectively (Fig. 10b and c). This study points out that, owing to the strong vertical pressure gradient, gas channels cannot coexist at the same time. In other words, only one gas channel can be active and expel gas at the surface at a given time.

Discussion

Seep site identification

The carbonate lenses of Beauvoisin were initially considered as pseudobioherms in the 1980s owing to their bioherm-like structure and composition (Gaillard *et al.* 1985). Although they contain reef-building organisms it is now considered that they did not form any significant relief on the seafloor (Gaillard *et al.* 1985; Rolin 1987; Peckmann *et al.* 1999; Gay 2002) even if some examples on modern sites show that they can form a positive relief above the seabed (Teichert *et al.* 2005; Himmler, *et al.* 2015). It has been shown that carbonate pavements formed *in situ* into the sediments (Bayon *et al.* 2009). The presence of autochthonous biological communities, together with a high density of one or very few taxa of chemotrophic megafauna, and lateral faunal gradients, are recognizable features of seep sites (Kauffman *et al.* 1996; Barbieri & Cavalazzi 2005). Moreover, the relation of fossil-rich carbonate lenses within the general stratigraphy and structural framework, their mineralogy and their geochemical features, including the biomarker signatures, are indicative of chemosynthetic organism activity (Campbell *et al.* 2002). Lucinid bivalves are the most prominent biota associated with the Oxfordian carbonate lenses, with some giant specimens, up to 15–20 cm in diameter, suggesting that they fed on abundant food and nutrients (Rolin 1987; Gay 2002). Detailed palaeoecology

studies indicate that the communities are similar to those of recent or present hydrothermal vents and cold seeps (Rolin *et al.* 1990; Gaillard *et al.* 1992) and to other fossil seep sites (Clari *et al.* 1994; Taviani 1994; Taylor & Glover 2009). More recently, geochemical analyses conducted on several Beauvoisin sub-sites have led to the conclusion that they were dependent on chemosynthesis (Peckmann *et al.* 1999; Tribovillard *et al.* 2013). The microbial oxidation of methane under anoxic conditions, referred to as sulphate-dependent anaerobic oxidation of methane (AOM), is a major biochemical process occurring at cold seeps. At sites where AOM is active, methane concentration varies strongly depending on spatial and temporal availability of methane supply and microbial turnover rates (Knittel & Boetius 2009; Deusner *et al.* 2014). Sulphate depletion is driven by methane oxidation in sediment pore-waters through bacterially mediated reactions, inducing a change in redox conditions (Feng & Roberts 2011) and favouring carbonate precipitation (Bayon *et al.* 2007; Ge *et al.* 2010; Vanneste *et al.* 2012, and references therein). At the Beauvoisin sub-sites the activity of sulphate-reducing bacteria is indicated first by the dispersively distributed framboidal pyrite within the nodules and by an outer rim of pyrite on the nodules (Gaillard *et al.* 1992; Gay 2002). Then, biomarkers of archaea were identified in Middle Oxfordian carbonate lenses, where methanogens produced heavy CO_2 leading to ^{13}C-enriched carbonate precipitation in the methanogenic zone with δ^{13}C values as high as +13 and 12.7‰ PDB (Peckmann *et al.* 1999; Tribovillard *et al.* 2013). The stable isotopic composition of carbonate lenses and nodules coupled with taxonomic endofauna shows that all sub-sites A–T located in the Beauvoisin anticline structure can be considered as cold seeps that developed within the sediment, near the sediment–water interface in a similar fashion to modern seep sites (Sibuet & Olu 1998; Campbell
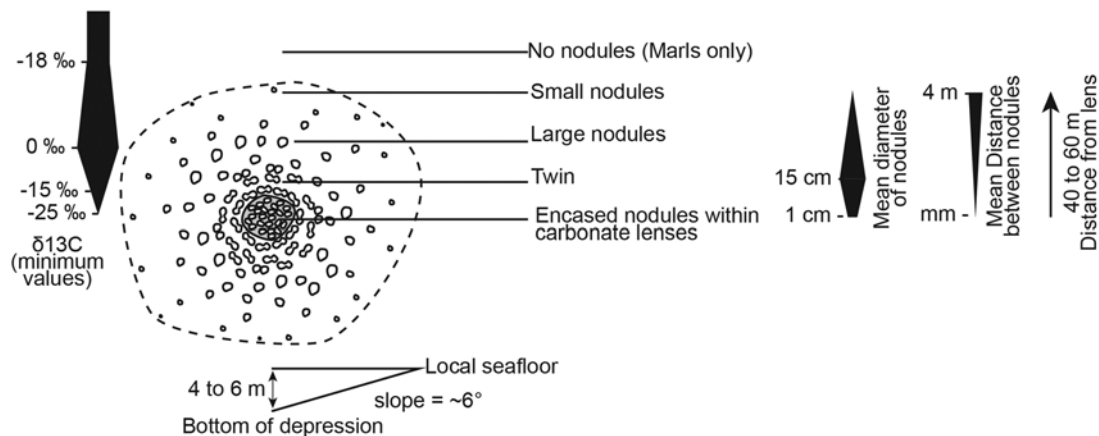
Fig. 11. Schematic diagram of the organization of a single carbonate lens located in the centre of an 80–120 m wide concentric area of nodules. Marker horizons on high-resolution logs allowed the identification of a 4–6 m deep depression with an average slope of about 6°, which is visually almost undetectable in the field.

2006; Bayon *et al.* 2007). This conclusion is also supported by specific enrichments in Mo, As and Sb in carbonate lenses, echoing the bacterially mediated formation of authigenic carbonate crusts through AOM (Tribovillard *et al.* 2013) as previously shown in the modern mud-volcano of the Malta Plateau (Cangemi *et al.* 2010).

Spatial organization

To better understand the spatial organization of a sub-site, the centrepiece is the nodule distribution and concentration. The size, shape and spatial organization of nodules at sub-sites A1–A3 are consistent with the observations made at sub-sites F and G (Figs 6 and 8), suggesting they have been formed through similar processes. These observations can be extended to almost all sub-sites, despite different outcrop conditions and forest cover. Only a few sub-sites seem not to be nodule-dependent, such as sub-sites L and M. These very close sub-sites (see Fig. 2 for location) mostly contain the irregular echinoid *Tithonia oxfordiana* (Gaillard *et al.* 1985, 1992, 2011; Senowbari-Daryan *et al.* 2007; Kiel 2010) and may represent some kind of exception as they do not contain a large macrofauna either.

The general organization of a single sub-site can be summarized as a set of vertically stacked carbonate lenses located in the centre of a concentric area of nodules. The basal lens is composed of a breccia made of mineralized veins, clasts-rich conduits crosscutting limestones and embedded nodules. This facies is similar to the 'brecciated limestone' from Italy (Ladanza *et al.* 2013), meaning that it may be due to an intense overpressured fluid flow affecting microbial carbonate and related macro-fauna in the subsurface, such as is observed in the injectite system of the Panoche Hills (Blouet *et al.* 2016). The carbonate lenses are interbedded with marls or claystones corresponding to varying fluxes of fluids such as in modern sites (Feng *et al.* 2010). The area affected by nodules is about 120 m wide forming a depression 4–6 m deep at a maximum compared with the regional stratigraphy as shown for sub-sites A1 and A2 (Figs 8 and 11). The average calculated slope is about 6°, which is visually almost undetectable in the field. Only high-resolution logs and the identification of marker horizons allow the identification of such low gradients.

Teachings from modern systems and sandbox modelling

Based on previous studies conducted on modern seep sites, particularly on the Regab pockmark in the Lower Congo Basin, we have shown that the centre of an active pockmark is not the main area for focused fluid seepage and the main point of emission may migrate laterally through time, forming new active sub-depressions

at the seafloor. Consequently, a giant pockmark is the result of the coalescence of successive seepage sub-areas forming a wide depression through time. This behaviour is confirmed in sandbox models, in which the walls of a feeding channel must collapse prior to the development of a new point of emission (Varas *et al.* 2015, and references therein). The main consequence is an intermittent fluid seep, although the fluid supply from deeper levels remains constant. This has also been documented in the Norway Basin, through the Giant Gjallar Vent (Gay *et al.* 2012; Dumke *et al.* 2014). In the light of observations made on the modern giant Regab pockmark and sandbox models, an intermittent fluid seep can also be interpreted in the Beauvoisin area. With respect to the stratigraphy some sub-sites can be grouped together as clusters (Fig. 12a). Seven clusters, C1–C7, were defined in the Beauvoisin area. Except for clusters C3 and C5 containing two sub-sites occurring at different positions at the same time, all other clusters are grouped in 200 m wide areas. This means that the point of fluid emission on the seabed has remained at almost the same geographical position for a significant period of time. A 3D view of the seven clusters shows that the system shifts in time from one cluster to the other (Fig. 12b). This also means that the occurrence of each cluster is separated from the next one by a period of relative quiescence during which no fluids (or only relict fluids) were expelled at the seabed. The durations of fluid seepage and fluid quiescence steps are variable. Given an estimated burial of 2000–2500 m for the Terres Noires Formation in the area (Gaillard *et al.* 1985; Rolin 1987), the compaction rate at the base and bottom of the composite log can be considered equivalent. In a first approximation, seven periods of active seafloor fluid seepage and eight periods of fluid quiescence alternated for 3.44 myr, corresponding to periods of 200 kyr each on average. However, at present the driving forces for focused fluid migration remain unclear. Major deep-rooted faults structuring the margin during the Oxfordian in the vicinity of the Beauvoisin area (in particular, the Propiac fault related to halokinesis; see Fig. 1 for location) may have played an efficient driving role for a long period of time, as suggested for other fossil seep sites (Aiello 2005). Finally, the Beauvoisin seep area can be considered as the result of clustered fluid seep sub-sites. This has led to the formation of an 800 m wide area of fluid seepage active for over 3.44 myr. In the light of this work, the Beauvoisin area can now be considered as a giant pockmark field.

Evolution model

Based on the comparison of fossil outcrop, modern and active pockmark, and sandbox model data, we propose here a new model
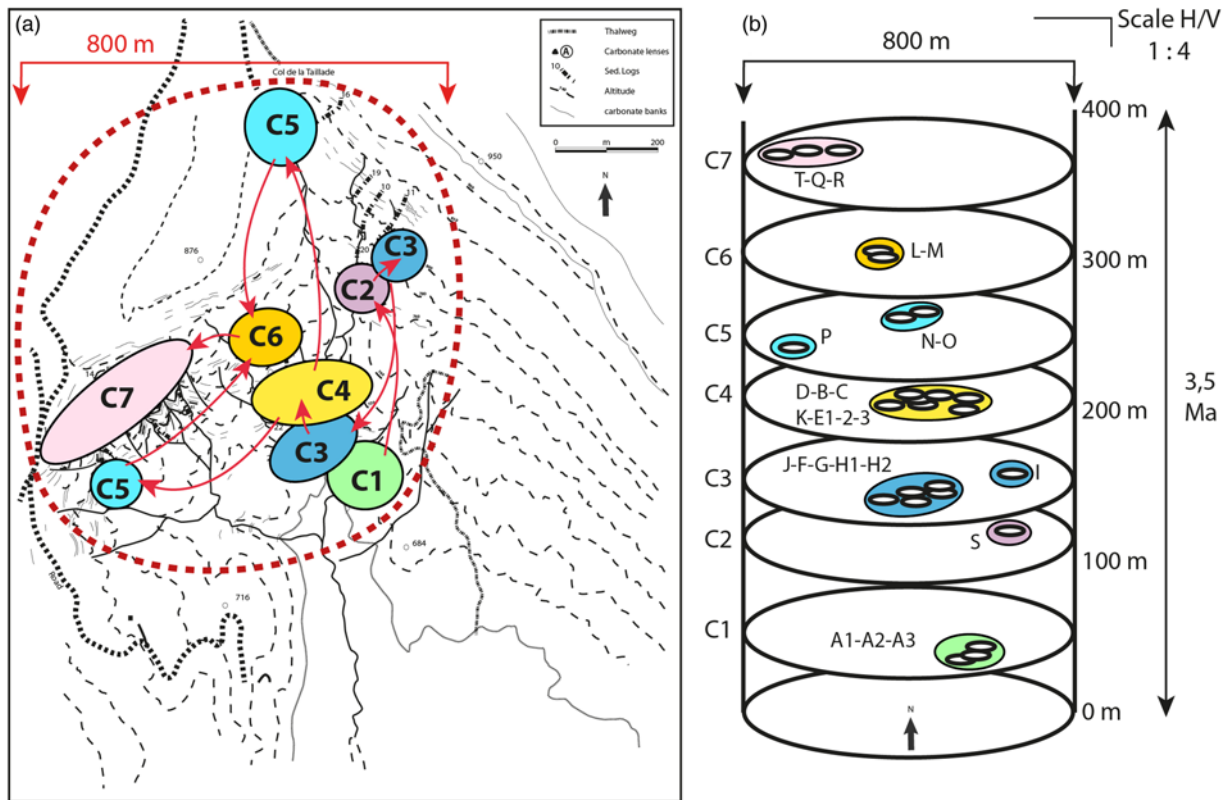
Fig. 12. (**a**) Map of the sub-sites A–T grouped by clusters regarding their stratigraphical and geographical positions in the Beauvoisin area. (**b**) Three-dimensional schematic view of the seven clusters showing that the point of emission at the seafloor has migrated laterally through time. The seven periods of active seafloor fluid seepage alternated with periods of fluid quiescence for about 3.4 myr, corresponding to periods of 200 kyr each on average. This means that all sub-sites A–T are genetically linked and they can be grouped in an 800 m wide giant pockmark.

for the internal evolution of a fluid seep area. Previous work conducted on sandbox models and numerical simulations have pointed out that, independently of the initial air invasion regime (percolation or fracture), similar systems develop a fluidized zone of parabolic shape characterized by a central air-channel, as described by Varas *et al.* (2011, 2015), Vidal *et al.* 2011; Ramos *et al.* (2015) and Poryles *et al.* (2016). These researchers showed that particles are intensively reworked within the parabolic area whereas particles do not have any movement outside of the parabolic area (Fig. 13a and b). This behaviour has been previously studied for hydraulic fractures, showing that they can occur without tectonic stresses (Mourgues *et al.* 2011), which is compatible with shallow unconsolidated and fluidized sediments. During the vertical growth of the hydraulic fracture, representing the fluid-channelling conduit, a cone of vertical upward displacements can be observed just above the tip of the fracture and the cone is limited by two large shear bands, indicating that the fracture opened exclusively in pure tension mode (Mourgues *et al.* 2012). This kind of cone deformation was observed in sedimentary basins, such as in the Norway Basin (Gay *et al.* 2012) or in the northern Mediteranean Sea (Gay *et al.* 2017), where the cone structure is accompanied by an uplift of the seabed, suggesting that this doming is the initial phase of fluid emission preceding a general collapse of the structure after which a pockmark forms. However, in the light of recent studies conducted on fluid flow through a water-saturated matrix of grains, such cone structures are most probably of parabolic shape (Poryles *et al.* 2016). A 2D seismic profile across the studied Regab giant pockmark field shows that reflections are very chaotic below the seabed (Fig. 13c). The disturbed zone is in fact parabolic in shape and is characterized by high-amplitude reflections that were interpreted as carbonate structures and/or gas-charged sediments (Gay 2002; Ondreas *et al.* 2005; Gay *et al.* 2006; Marcon *et al.*

2014). The base of the parabolic area is clearly located on top of a vertically fractured zone that is usually interpreted as a seismic pipe (Gay *et al.* 2006; Løseth *et al.* 2011; Ho *et al.* 2012), very similar to the structure found further north in the Lower Congo Basin at the Hydrate Hole, where the deformed zone in the subsurface is located directly above an underlying fault clearly visible on seismic sections (Wenau *et al.* 2017). Previous studies conducted in the Norway Basin have also documented V-shaped anomalies beneath pockmarks corresponding to the transition from focused to distributed fluid flow (Betzler *et al.* 2011; Gay *et al.* 2012). This seismic facies appears as a 'flower' structure with a vertical narrow zone considered as the stem (i.e. the pipe) feeding a wide area considered as the corolla (i.e. the disturbed sediments) (Gay *et al.* 2012). It can be interpreted as deformation of cohesionless, unlithified sediments caused by fluid injection (Gay *et al.* 2017).

We propose here a simple model of a giant fossil pockmark considered as an outcrop analogue to modern giant pockmarks (Fig. 13d). Based on previous studies the V-shaped anomaly (Gay *et al.* 2012), or the cone-in-cone structure (Mourgues *et al.* 2012), is more probably parabolic in shape. However, to date in the fossil pockmark of Beauvoisin, neither the point of injection (i.e. the base of the parabolic area) nor the fluid pipes are clearly identified (Fig. 13d). This is probably due to outcrop conditions, the Beauvoisin area being located in the heart of an eroded east–west anticline structure with dense forest cover. The measured values of $\delta^{13}C$ and the presence of *n*-alkanes in the hydrocarbon fraction of veins and nodules thus correspond to a contribution of different sources of carbon including a methane thermogenic origin from thermal maturation of organic matter at the base of the Terres Noires Formation or below it (Peckmann & Thiel 2004). This observation, coupled with fluid migration being active for at least 3.4 myr, suggests that a significant amount of fluids migrated during this
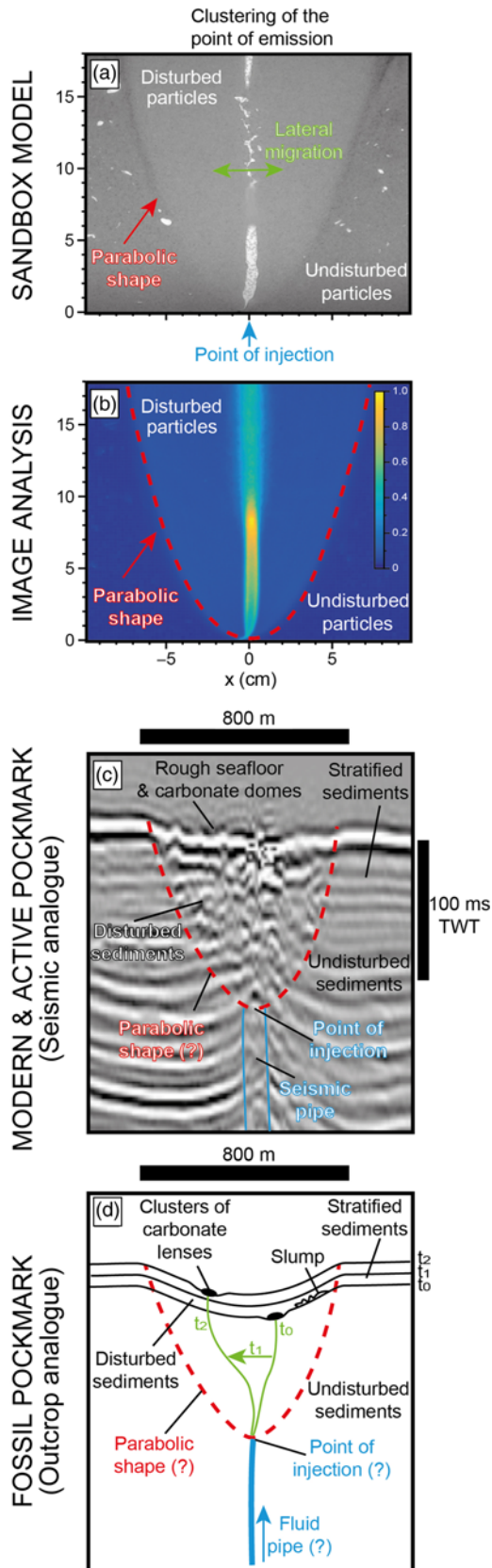
Fig. 13. (**a**) Two-dimensional sandbox experiment of air injection in a Hele–Shaw cell filled with water-saturated grains ($d = 318 \pm 44$ μm, $h_g = 20$ cm, $h_w = 2$ cm, $\Phi = 0.66$ ml s^{-1}). The zone where the sediments are disturbed has a roughly parabolic shape (in red), and the central gas channel displays erratic lateral motion in time (in green), leading to lateral variations of emission of bubbles at the surface. (**b**) Normalized flow density (indicated by the colour-bar) computed for the series of images from which (**a**) is extracted. High values of the flow density indicate regions where motion occurred in the system.

Fig. 13. *Continued.* This analysis reveals the parabolic shape of the disturbed zone (in red). (**c**) Two-dimensional seismic profile of the Regab giant pockmark showing a disturbed zone directly beneath the main depression (modified after Gay *et al.* 2006). The limit between undisturbed reflections and the chaotic reflections is parabolic in shape (in red). The base of the parabolic area is located on top of a vertically fractured zone (in blue) that is usually interpreted as a seismic pipe, playing the role of a feeder conduit for fluids. This facies is called a 'flower' structure, with a vertical narrow zone considered as the stem (i.e. the seismic pipe) feeding a wide area considered as the corolla (i.e. the disturbed sediments). (**d**) Model of the Beauvoisin seep site considered as an outcrop analogue for a giant pockmark. In the main depression, carbonate lenses are organized in clusters that have migrated laterally through time. At time t_0 the first cluster is fed by an irregular conduit (green line). During time t_1 the conduit has collapsed, laterally shifted and reopened at a different location feeding a new cluster of carbonate lenses during time t_2. This means that even if a pockmark seems dead or inactive, it could be at stage t_1 corresponding to the period of shifting of the feeding conduit in the disturbed zone. However, at present neither the parabolic shape of the disturbed zone (in red), nor the feeding conduits at depth (in blue) have been identified yet.

period. However, it does not mean that the fluid flow in the subsurface is constant over time. On modern sites varying fluid flows were documented in the subsurface, producing authigenic high-Mg calcite or aragonite depending on the CH_4 flux rate and forming pavements or concretions (Nöthen & Kasten 2011). If the flux rate is not high enough, only disseminated concretions precipitated. At a specific point of emission, the fluid flux in the shallow subsurface is not high enough to sustain massive carbonate precipitation, but this does not mean that the fluid flux is also reduced at depth. In the disturbed zone, carbonate lenses are organized in clusters that migrate laterally through time. At time t_0 the first cluster is fed by an irregular conduit (green line in Fig. 13d). Time t_1 corresponds to the time necessary for the conduit to collapse, then to shift laterally and then to open at a different location. The time t_2 corresponds to the birth of a new cluster of carbonate lenses. Based on the detailed stratigraphy we showed that the times t_0, t_1 and t_2 are relatively equivalent in terms of duration, about 200 kyr each. This means that even if a pockmark seems dead and inactive, it could be at stage t_1, corresponding to a shift of the feeding conduit in the disturbed zone. As observed in both modern and fossil fluid seep areas, a long-lasting fluid migration is channelized through focused structures (Løseth *et al.* 2011; Ho *et al.* 2012) that could constantly feed the disturbed zone. The next challenge in the area will be to identify such underlying pipe structures, as the bitumen infilling of veins and nodules may correspond to a later stage of heavier fluid migration as shown for the 'Brecciated Limestone' in Italy (i.e. secondary migration in the petroleum system; Ladanza *et al.* 2015). In the case of the Beauvoisin seep site, this would mean that the feeding pipes remained open for a long period of time.

Conclusion

For over 30 years, a fluid seep system has been known in the Beauvoisin area, located on the Jurassic passive margin of the SE Basin of France (Gaillard *et al.* 1985). Modern marine investigations coupled with sandbox models permitted comparison of the architecture of the Beauvoisin seep site with an active fluid seep area on the modern passive margin of the Lower Congo Basin. The main conclusion is that they have very similar features although they do not occur at the same geological time. In the same way, the sandbox models of fluid injection structures have shown that the involved processes have led to a similar organization in three dimensions, in particular in terms of the following aspects.

(1) Stratigraphy. Based on 23 sedimentological sections in the Beauvoisin area, 19 sub-sites A–T have been reported in a composite log, representing a total thickness of about 370 m. As a result of weathering and erosion since the site discovery, two new sub-sites S and T were identified and integrated in the general log, based on the initial nomenclature established by Rolin (1987).

(2) Sub-site shape and organization. Each identified sub-site is composed of subvertically stacked carbonate lenses. Detailed logs at various distances from the vertical axis of carbonate lenses have shown that the sub-sites developed in smooth depressions, 4–6 m deeper than the surrounding seabed. Nodules are present within the depression only. They are encased in the carbonate lenses in the centre whereas their size varies depending on the distance from the centre. Coupled with the varying $\delta^{13}C$ values, this indicates that nodules can be considered as markers of a sub-site, even if outcrop conditions do not allow identification of carbonate lenses buried in marls.

(3) General organization. The carbonate lenses are organized in clusters of up to seven sub-sites grouped together in the same stratigraphic interval and the same geographical zone within the seeping area. Only a few sub-sites seem active at the same time in a given cluster. The coalescence of all clusters leads to the formation of a wide depression. This general organization is very similar to that of the modern Regab giant pockmark field in the Lower Congo Basin. The seep site of Beauvoisin can be clearly considered as a fossil giant pockmark field, analoguous to pockmarks in modern basins.

(4) Timing. A detailed stratigraphic correlation coupled with extensive mapping of fluid seep sub-sites in the Beauvoisin area has led to a spatio-temporal 3D reconstruction of the position of these sub-sites. This shows that periods of fluid seeping alternated with periods of apparent quiescence, about 200 kyr each.

A pockmark is a seafloor depression hosting seep sites, both active and inactive. The study of the modern Regab pockmark shows that it is formed by the coalescence of smaller depressions, each about 100 m wide. However, submersible dives and gravity cores provide only a partial vision of the seafloor without integrating the sub-seafloor and the connection with fluid pipes at depth. A way to access the pockmark underground is by studying outcrop analogues, such as the Beauvoisin giant pockmark. The study of this site provided a real breakthrough in the understanding of fluid activity in the disturbed zone below the seafloor. The main result is that a pockmark could seem inactive for a long period of time owing to the lateral shift of the feeder conduit, meaning that the sub-seafloor remains charged in gas. This observation will be of great importance in the geobiology of fluid seeps (Peckmann 2005; Judd & Hovland 2007), in risk assessment for anthropic activities at the sea-bottom (Gay et al. 2017) and for hydrocarbon exploration (Capozzi et al. 2017).

Scientific editing by Adrian Hartley

References

Agirrezabala, L.M., Kiel, S., Blumenberg, M., Schäfer, N. & Reitner, J. 2013. Outcrop analogues of pockmarks and associated methane-seep carbonates: A case study from the Lower Cretaceous (Albian) of the Basque–Cantabrian Basin, western Pyrenees. *Palaeogeography, Palaeoclimatology, Palaeoecology*, **390**, 94–115.

Aiello, I.W. 2005. Fossil seep structures of the Monterey Bay region and tectonic/structural controls on fluid flow in an active transform margin. *Palaeogeography, Palaeoclimatology, Palaeoecology*, **227**, 124–142.

Aloisi, G., Pierre, C., Rouchy, J.M., Foucher, J.P. & Woodside, J. 2000. Methane-related authigenic carbonates of eastern Mediterranean Sea mud volcanoes and their possible relation to gas hydrate destabilisation. *Earth and Planetary Science Letters*, **184**, 321–338.

Aloisi, G., Bouloubassi, I. *et al.*, 2002. CH_4-consuming microorganisms and the formation of carbonate crusts at cold seeps. *Earth and Planetary Science Letters*, **203**, 195–203.

Amano, K., Jenkins, R.G., Aikawa, M. & Nobuhara, T. 2010. A Miocene chemosynthetic community from the Ogaya Formation in Joetsu: Evidence for depth-related ecologic control among fossil seep communities in the Japan Sea back-arc basin. *Palaeogeography, Palaeoclimatology, Palaeoecology*, **286**, 164–170.

Artru, P. 1972. *Les Terres Noires du bassin rhodanien (Bajocien supérieur à Oxfordien moyen). Stratigraphie – Sédimentologie – Géochimie*. Thèse d'Etat, Université de Lyon.

Barbieri, R. & Cavalazzi, B. 2005. Microbial fabrics from Neogene cold seep carbonates, Northern Apennine, Italy. *Palaeogeography, Palaeoclimatology, Palaeoecology*, **227**, 143–155.

Bayon, G., Pierre, C., *et al.* 2007. Sr/Ca and Mg/Ca ratios in Niger Delta sediments: implications for authigenic carbonate genesis in cold seep environments. *Marine Geology*, **241**, 93–109.

Bayon, G., Henderson, G.M. & Bohn, M. 2009. U–Th stratigraphy of a cold seep carbonate crust. *Chemical Geology*, **260**, 47–56.

Beauchamp, B. & Savard, M.M. 1992. Cretaceous Chemosynthetic Carbonate Mounds in the Canadian Arctic. *Palaios*, **7**, 434, https://doi.org/10.2307/3514828

Betzler, C., Lindhorst, S., Hübscher, C., Lüdmann, T., Fürstenau, J. & Reijmer, J. 2011. Giant pockmarks in a carbonate platform (Maldives, Indian Ocean). *Marine Geology*, **289**, 1–16.

Blouet, J.-P., Imbert, P. & Foubert, A. 2016. Mechanisms of biogenic gas migration revealed by seep carbonate paragenesis, Panoche Hills, California. *AAPG Bulletin*, **101**, 1309–1340.

Boetius, A., Ravenschlag, K., *et al.* 2000. A marine microbial consortium apparently mediating anaerobic oxidation of methane. *Nature*, **407**, 623–626.

Bohrmann, G., Greinert, J., Suess, E. & Torres, M. 1998. Authigenic carbonates from the Cascadia subduction zone and their relation to gas hydrate stability. *Geology*, **26**, 647–650.

Brooks, M.C., Wise, W.R. & Annable, M.D. 1999. Fundamental changes in *in-situ* air sparging flow patterns. *Groundwater Monitoring and Remediation*, **19**, 105–113, https://doi.org/10.1111/j.1745-6592.1999.tb00211.x

Campbell, K.A. 2006. Hydrocarbon seep and hydrothermal vent paleoenvironments and paleontology: past developments and future research directions. *Palaeogeography, Palaeoclimatology, Palaeoecology*, **232**, 362–407.

Campbell, K.A. & Bottjer, D.J. 1995*a*. Brachiopods and chemosymbiotic bivalves in Phanerozoic hydrothermal vent and cold seep environments. *Geology*, **23**, 321–324.

Campbell, K.A. & Bottjer, D.J. 1995*b*. *Peregrinella*: an Early Cretaceous cold-seep-restricted brachiopod. *Paleobiology*, **24**, 461–478.

Campbell, K.A., Farmer, J.D. & Des Marais, D. 2002. Ancient hydrocarbon seeps from the Mesozoic convergent margin of California: carbonate geochemistry, fluids and palaeoenvironments. *Geofluids*, **2**, 63–94.

Cangemi, M., Di Leonardo, R., Bellanca, A., Cundy, A., Neri, R. & Angelone, M. 2010. Geochemistry and mineralogy of sediments and authigenic carbonates from the Malta Plateau, Strait of Sicily (Central Mediterranean): relationships with mud/fluid release from a mud volcano system. *Chemical Geology*, **276**, 294–308.

Capozzi, R., Oppo, D. & Taviani, M. 2017. Cold seepages: An economic tool for hydrocarbon appraisal. *AAPG Bulletin*, **101**, 617–623.

Casenave, V., Gay, A. & Imbert, P. 2017. Spider structures: records of fluid venting from methane hydrates on the Congo continental slope. *Bulletin de la Société Géologique de France*, **188**, E3.

Clari, P., Fornara, L., Ricci, B. & Zuppi, G.M. 1994. Methane-derived carbonates and chemosymbiotic communities of Piedmont (Miocene, northern Italy): an update. *Geo-Marine Letters*, **14**, 201–209.

Claypool, G.E., Holser, W.T., Kaplan, I.R., Sakai, H. & Zak, I. 1980. The age curves of sulphur and oxygen isotopes in marine sulphate and their interpretation. *Chemical Geology (Isotope Geoscience Section)*, **28**, 199–260.

A. Gay *et al.*

Craig, H. & Gordon, I. 1965. Deuterium and oxygen-18 variations in the ocean and marine atmosphere. *In*: Tongiorgi, E. (ed.) *Stable Isotopes in Oceanographic Studies and Paleotemeratures*. Consiglio Nazionale delle Richerche, Laboratorio di Geologia Nucleare, Pisa, 9–130.

Dardeau, G. 1988. Tethyan evolution and Alpine reactivation of Jurassic extensional structures in the French 'Alpes Maritimes'. *Bulletin de la Société Géologique de France*, **8**, 651–657.

Deusner, C., Holler, T., Arnold, G.L., Bernasconi, S.M., Formolo, M.J. & Brunner, B. 2014. Sulfur and oxygen isotope fractionation during sulfate reduction coupled to anaerobic oxidation of methane is dependent on methane concentration. *Earth and Planetary Science Letters*, **399**, 61–73.

Dumke, I., Berndt, C., Crutchley, G.J., Krause, S., Liebetrau, V., Gay, A. & Couillard, M. 2014. Seal bypass at the Giant Gjallar Vent (Norwegian Sea): Indications for a new phase of fluid venting at a 56-Ma-old fluid migration system. *Marine Geology*, **351**, 38–52.

Feng, D. & Roberts, H.H. 2011. Geochemical characteristics of the barite deposits at cold seeps from the northern Gulf of Mexico continental slope. *Earth and Planetary Science Letters*, **309**, 89–99.

Feng, D., Chen, D., Peckmann, J. & Bohrmann, G. 2010. Authigenic carbonates from methane seeps of the northern Congo fan: microbial formation mechanism. *Marine and Petroleum Geology*, **27**, 748–756.

Gaidon, J.L., Martin-Calle, S. & Boudeulle, M. 1988. Pyrite from concretion pipes in mesozoic shales: mineralogical and chemical evidence of hydrothermal origin. *Marine Geology*, **84**, 239–256.

Gaillard, C. & Rolin, Y. 1988. Relation entre tectonique synsédimentaire et pseudobioherms (Oxfordien de Beauvoisin – Drôme – France). Un argument supplémentaire pour interpréter les pseudobioherms comme formés au droit de sources sous-marines. *Comptes Rendus de l'Académie des Sciences*, **307**, 1265–1270.

Gaillard, C., Bourseau, J.P., Boudeulle, M., Pailleret, P., Rio, M. & Roux, M. 1985. Les pseudobioherms de Beauvoisin (Drôme): un site hydrothermal sur la marge téthysienne l'Oxfordien? *Bulletin de la Société Géologique de France, Série 8*, **1**, 69–78.

Gaillard, C., Rio, M., Rolin, Y. & Roux, M. 1992. Fossil chemosynthetic communities related to vents or seeps in sedimentary basins: the pseudobioherms of southeastern France compared to other world examples. *Palaios*, **7**, 451–465.

Gaillard, C., Atrops, F., *et al.* 1996. Description stratigraphique préliminaire des faisceaux alternants de l'Oxfordien moyen dans le bassin dauphinois (Sud-Est de la France). *Géologie de la France*, **1**, 17–24.

Gaillard, C., Neraudeau, D. & Thierry, J. 2011. *Tithonia oxfordiana*, a new irregular echinoid associated with Jurassic seep deposits in South-East France. *Palaeontology*, **54**, 735–752.

Gay, A. 2002. Les marqueurs géologiques de la migration et de l'expulsion des fluides sédimentaires sur le plancher des marges passives matures. Exemples dans le Bassin du Congo. PhD thesis, Université de Lille 1.

Gay, A. & Migeon, S. 2017. Geological fluid flow in sedimentary basins. *Bulletin de la Société Géologique de France*, **188**, 1–6, https://doi.org/10.1051/bsgf/2017200

Gay, A., Lopez, M., Ondreas, H., Charlou, J.-L., Sermondadaz, G. & Cochonat, P. 2006. Seafloor facies related to upward methane flux within a Giant Pockmark of the Lower Congo Basin. *Marine Geology*, **226**, 81–95.

Gay, A., Lopez, M., Berndt, C. & Séranne, M. 2007. Geological controls on focused fluid flow associated with seafloor seeps in the Lower Congo Basin. *Marine Geology*, **244**, 68–92.

Gay, A., Mourgues, R., *et al.* 2012. Anatomy of a fluid pipe in the Norway Basin: initiation, propagation and 3D shape. *Marine Geology*, **332–334**, 75–88.

Gay, A., Cavailhes, T., Grauls, D., Marsset, B. & Marsset, T. 2017. Repeated fluid expulsions during events of rapid sea-level rise in the Gulf of Lion, western Mediterranean Sea. *Bulletin de la Société Géologique de France*, **188**, https://doi.org/10.1051/bsgf/2017190

Ge, L., Jiang, S.-Y., *et al.* 2010. Chemical environment of cold seep carbonate formation on the northern continental slope of South China Sea: Evidence from trace and rare earth element geochemistry. *Marine Geology*, **277**, 21–30.

Gradstein, J.G., Ogg, J.G., Schmitz, M.D. & Ogg, G.M. 2012. (eds) *The Geologic Time Scale 2012*. Elsevier, Amsterdam.

Greinert, J., Bohrmann, G. & Suess, E. 2001. Gas hydrate-associated carbonates and methane-venting at Hydrate Ridge: classification, distribution and origin of authigenic lithologies. *In*: Paull, C.K. & Dillon, W.P. (eds) *Natural Gas Hydrates: Occurrence, Distribution, and Detection*, AGU Geophysical Monograph Series, **124**, 99–123.

Haas, A., Peckmann, J., Elvert, M., Sahling, H. & Bohrmann, G. 2010. Patterns of carbonate authigenesis at the Kouilou pockmarks on the Congo deep-sea fan. *Marine Geology*, **268**, 129–136.

Han, X., Suess, E., Sahling, H. & Wallmann, K. 2004. Fluid venting activity on the Costa Rica margin: new results from authigenic carbonates. *International Journal of Earth Sciences*, **93**, 596–611.

Himmler, T., Birgel, D., Bayon, G., Pape, T., Ge, L., Bohrmann, G. & Peckmann, J. 2015. Formation of seep carbonates along the Makran convergent margin, northern Arabian Sea and a molecular and isotopic approach to constrain the carbon isotopic composition of parent methane. *Chemical Geology*, **415**, 102–117.

Ho, S., Cartwright, J.A. & Imbert, P. 2012. Vertical evolution of fluid venting structures in relation to gas flux, in the Neogene–Quaternary of the Lower Congo Basin, Offshore Angola. *Marine Geology*, **332**, 40–55.

Ingrassia, M., Martorelli, E., Bosman, A., Macelloni, L., Sposato, A. & Chiocci, F.L. 2015. The Zannone Giant Pockmark: First evidence of a giant complex seeping structure in shallow-water, central Mediterranean Sea, Italy. *Marine Geology*, **363**, 38–51.

Judd, A. & Hovland, M. 2007. *Seabed Fluid Flow, the Impact on Geology, Biology and the Marine Environment*. Cambridge University Press, Cambridge, 290–314.

Kauffman, E.G., Arthur, M.A., Howe, B. & Scholle, P.A. 1996. Widespread venting of methane-rich fluids in Late Cretaceous (Campanian) submarine springs (Tepee Buttes), Western Interior seaway, U.S.A. *Geology*, **24**, 799–802.

Kiel, S. 2010. The fossil record of vent and seep mollusks. *In*: Kiel, S. (ed.) *The Vent and Seep Biota: Aspects from Microbes to Ecosystems*. Topics in Geobiology, **33**. Springer, Heidelberg, 255–278.

Kiel, S. 2013. Lucinid bivalves from ancient methane seeps. *Journal of Molluscan Studies*, **79**, 346–363, https://doi.org/10.1093/mollus/eyt035

Kiel, S. & Little, C.T.S. 2006. Cold seep mollusks are older than the general marine mollusk fauna. *Science*, **313**, 1429–1431.

Knittel, K. & Boetius, A. 2009. Anaerobic oxidation of methane: progress with an unknown process. *Annual Review of Microbiology*, **63**, 311–344.

Ladanza, A., Sampalmieri, G., Cipollari, P., Mola, M. & Cosentino, D. 2013. The 'Brecciated Limestones' of Maiella, Italy: Rheological implications of hydrocarbon-charged fluid migration in the Messinian Mediterranean Basin. *Palaeogeography, Palaeoclimatology, Palaeoecology*, **390**, 130–147.

Ladanza, A., Sampalmieri, G. & Cipollari, P. 2015. Deep-seated hydrocarbons in the seep 'Brecciated Limestones' of the Maiella area (Adriatic foreland basin): Evaporitic sealing and oil re-mobilization effects linked to the drawdown of the Messinian Salinity Crisis. *Marine and Petroleum Geology*, **66**, 177–191.

Lemoine, M. 1985. Structuration jurassique des Alpes occidentales et palinspatique de la Téthys ligure. *Bulletin de la Société Géologique de France*, **I**, 126–137.

Lemoine, M., Arnaud-Vanneau, A., Arnaud, H., Létolle, R., Mével, C. & Thieuloy, J.P. 1982. Indices possibles de paléo-hydrothermalisme marin dans le Jurassique et le Crétacé des Alpes occidentales (océan téthysien et sa marge continentale européenne): essai d'inventaire. *Bulletin de la Société Géologique de France*, **S7-XXIV**, 641–647, https://doi.org/10.2113/gssgfbull.S7-XXIV.3.641

Løseth, H., Wensaas, L. *et al.* 2011. 1000 m long gas blow-out pipes. *Marine and Petroleum Geology*, **28**, 1047–1060.

Louis-Schmid, B., Rais, P., Logvinovich, D., Bernasconi, S.M. & Weissert, H. 2007. Impact of methane seeps on the local carbon-isotope record: a case study from a Late Jurassic hemipelagic section. *Terra Nova*, **19**, 259–265.

Loyd, S.J. & Berelson, W.M. 2015. The modern record of 'concretionary' carbonate: Reassessing a discrepancy between modern sediments and the geologic record. *Chemical Geology*, **420**, 77–87.

Marcon, Y., Ondréas, H., Sahling, H., Bohrmann, G. & Olu, K. 2014. Fluid flow regimes and growth of a giant pockmark. *Geology*, **42**, 63–66.

Mascle, G. 1988. Salt tectonics, Tethyan rifting and Alpine folding in the French Alps. *Bulletin de la Société Géologique de France*, **8**, 747–758.

Mourgues, R., Gressier, J.B., Bodet, L., Bureau, D. & Gay, A. 2011. 'Basin scale' versus 'localized' pore pressure/stress coupling: Implications for trap integrity evaluation. *Marine and Petroleum Geology*, **28**, 1111–1121.

Mourgues, R., Bureau, D., Bodet, L., Gay, A. & Gressier, J. 2012. Formation of conical fractures in sedimentary basins: Experiments involving pore fluids and implications for sandstone intrusion mechanisms. *Earth and Planetary Science Letters*, **313**, 67–78.

Natalicchio, M., Peckmann, J., Birgel, D. & Kiel, S. 2015. Seep deposits from northern Istria, Croatia: a first glimpse into the Eocene seep fauna of the Tethys region. *Geology Magazine*, **152**, 444–459.

Nöthen, K. & Kasten, S. 2011. Reconstructing changes in seep activity by means of pore water and solid phase Sr/Ca and Mg/Ca ratios in pockmark sediments of the Northern Congo Fan. *Marine Geology*, **287**, 1–13.

Ondreas, H., Charlou, J.-L., *et al.* 2005. Integrated '*in situ*' study of a deep giant pockmark on the Congo–Angola margin. *Geo-Marine Letters*, **25**, 281–292.

Paull, C.K., Chanton, J.P., Neumann, A.C., Coston, J.A., Martens, C.S. & Showers, W. 1992. Indicators of methane-derived carbonates and chemosynthetic organic carbon deposits: examples from the Florida escarpment. *Palaios*, **7**, 361–375.

Peckmann, J. 2005. Geobiology of ancient and modern methane seeps. *Palaeogeography, Palaeoclimatology, Palaeoecology*, **227**, 1–5.

Peckmann, J. & Thiel, V. 2004. Carbon cycling at ancient methane-seeps. *Chemical Geology*, **205**, 443–467.

Peckmann, J., Thiel, V., Michaelis, W., Clari, P., Gaillard, C., Martire, L. & Reitner, J. 1999. Cold seep deposits of Beauvoisin (Oxfordian; southeastern France) and Marmorito (Miocene; northern Italy): microbially induced authigenic carbonates. *International Journal of Earth Sciences*, **88**, 60–75.

Pellenard, P., Deconinck, J.F., Marchand, D., Thierry, J., Fortwengler, D. & Vigneron, G. 1999. Contrôle géodynamique de la sédimentation argileuse du Callovien–Oxfordien moyen dans l'Est du Bassin de Paris: influence eustatique et volcanique. *Comptes Rendus de l'Académie des Sciences*, **328**, 807–813.

Pellenard, P., Deconinck, J.F., Huff, W.D., Thierry, J., Marchand, D. & Trouiller, A. 2003. Characterisation and correlation of Upper Jurassic (Oxfordian) bentonite deposits of the Paris Basin and the South-Eastern Basin of France. *Sedimentology*, **50**, 1035–1060.

Poryles, R., Vidal, V. & Varas, G. 2016. Bubbles trapped in a fluidized bed: trajectories and contact area. *Physical Review E*, **93**, 032904.

Ramos, G., Varas, G., Géminard, J.-C. & Vidal, V. 2015. Gas-induced fluidization of mobile liquid-saturated grains. *Physical Review E*, **92**, 062210.

Roberts, H.H., Aharon, P. & Walsh, M.M. 1993. Cold-seep carbonates of the Louisiana continental slope-to-basin floor. *In:* Rezak, R. & Lavoie, D.L. (eds) *Carbonate microfabrics*. Springer-Verlagp. 95–104.

Rolin, Y. 1987. Gisements fossilifères liés à des sources sous-marines dans le bassin des Terres Noires: le site oxfordien de Beauvoisin (Drôme, Chaînes subalpines méridionales), Comparaison avec les sites océaniques actuels. Thèse de doctorat, Université de Lyon.

Rolin, Y., Gaillard, C. & Roux, M. 1990. Ecologie des pseudobiohermes des Terres Noires jurassiques liés à des paléo-sources sous-marines. Le site oxfordien de Beauvoisin (Drôme, Bassin du Sud-Est, France). *Paleogeography, Palaeoclimatology, Palaeoecology*, **80**, 79–105.

Selker, J.S., Niemet, M., McDuffie, N.G., Gorelick, S.M. & Parlange, J.Y. 2007. The local geometry of gas injection into saturated homogeneous porous media. *Transport in Porous Media*, **68**, 107–127, https://doi.org/10.1007/s11242-006-0005-0

Senowbari-Daryan, B., Gaillard, C. & Peckmann, J. 2007. Crustacean microcoprolites from Jurassic (Oxfordian) hydrocarbon-seep deposits of Beauvoisin, southeastern France. *Facies*, **53**, 229–238.

Sibuet, M. & Olu, K. 1998. Biogeography, biodiversity and fluid dependence of deep-sea cold-seep communities at active and passive margins. *Deep-Sea Research II*, **45**, 517–567.

Stewart, S.A. 2015. Circular geological structures outcropping in the sedimentary basins of Saudi Arabia. *Journal of Asian Earth Sciences*, **106**, 95–118.

Taviani, M. 1994. The 'calcari a Lucina' macrofauna reconsidered: Deep-sea faunal oases from Miocene-age cold vents in the Romagna Apennine, Italy. *Geo-Marine Letters*, **14**, 185–191.

Taylor, J.D. & Glover, E.A. 2009. A giant lucinid bivalve from the Eocene of Jamaica – Systematics, life habits and chemosymbiosis (Mollusca: bivalvia: Lucinidae). *Palaeontology*, **52**, 95–109.

Teichert, B.M.A. & van de Schootbrugge, B. (ed.) 2013. *Tracing Phanerozoic hydrocarbon seepage from local basins to the global Earth system*. Elsevier, Amsterdam, https://doi.org/10.1016/j.palaeo.2013.10.001

Teichert, B.M.A., Bohrmann, G. & Suess, E. 2005. Chemoherms on Hydrate Ridge – Unique microbially-mediated carbonate build-ups growing into the water column. *Palaeogeography, Palaeoclimatology, Palaeoecology*, **227**, 67–85.

Tribovillard, N., Armynot du Châtelet, E., Gay, A., Barbecot, F., Sansjofre, P. & Potdevin, J.-L. 2013. Geochemistry of cold seepage-impacted sediments: per-ascensum or per-descensum trace metal enrichment? *Chemical Geology*, **340**, 1–12.

Vanneste, H., Kastner, M., *et al.* 2012. Authigenic carbonates from the Darwin Mud Volcano, Gulf of Cadiz: a record of palaeo-seepage of hydrocarbon bearing fluids. *Chemical Geology*, **300–301**, 24–39.

Varas, G., Vidal, V. & Géminard, J.-C. 2011. Venting dynamics of an immersed granular layer. *Physical Review E*, **83**, 011302.

Varas, G., Ramos, G., Géminard, J.-C. & Vidal, V. 2015. Flow and fracture in water-saturated, unconstrained granular beds. *Frontiers of Physics*, **3**, 44.

Vidal, V., Varas, G. & Géminard, J.-C. 2010. Dynamique de dégazage dans un milieu granulaire immergé: différents aspects. *In*: Josserand, C., Lefranc, M. & Letellier, C. (eds) *Compte-rendus de la 13e Rencontre du Non-Linéaire*. Non-Linéaire Publications, Orsay, France, 199–204.

Vidal, V., Varas, G. & Géminard, J.-C. 2011. 'Venting' dans un milieu granulaire immergé. *In*: Josserand, C., Lefranc, M. & Letellier, C. (eds) *Compte-rendus de la 14e Rencontre du Non-Linéaire*. Non-Linéaire Publications, Orsay, France, 175–180.

Vrijenhoeck, R.C. 2013. On the instability and evolutionary age of deep-sea chemosynthetic communities. *Deep-Sea Research II*, **92**, 189–200.

Wenau, S., Spieß, V., Pape, T. & Fekete, N. 2017. Controlling mechanisms of giant deep water pockmarks in the Lower Congo Basin. *Marine and Petroleum Geology*, **83**, 140–157.

Whiticar, M.J. 1999. Carbon and hydrogen isotope systematics of bacterial formation and oxidation of methane. *Chemical Geology*, **161**, 291–314.